BNL-79479-2007-BC

Metal Oxide Nanoparticles

Marcos Fernández-Garcia, José A. Rodriguez

To be published in "Nanomaterials: Inorganic and Bioinorganic Perspectives"

October 2007

Chemistry Department

Brookhaven National Laboratory
P.O. Box 5000
Upton, NY 11973-5000
www.bnl.gov

DISCLAIMER

BNL-79479-2007-BC

METAL OXIDE NANOPARTICLES

Marcos Fernández-García[a] *and José A. Rodriguez*[b]

[a] Instituto de Catálisis y Petroleoquímica, CSIC, C/Marie Curie 2, Cantoblanco, 28049-Madrid, Spain

[b] Department of Chemistry, Brookhaven National Laboratory, Upton, NY 11973, USA

Emails: mfg@icp.csic.es; rodrigez@bnl.gov

Abstract

This chapter covers the fundamental science, synthesis, characterization, physico-chemical properties and applications of oxide nanomaterials. Explains fundamental aspects that determine the growth and behavior of these systems, briefly examines synthetic procedures using bottom-up and top-down fabrication technologies, discusses the sophisticated experimental techniques and state of the art theory results used to characterize the physico-chemical properties of oxide solids and describe the current knowledge concerning key oxide materials with important technological applications.

Keywords

Oxides; Al_2O_3, MgO; ZrO_2; CeO_2, TiO_2; ZnO; Fe_2O_3; SnO; structural and electronic properties; physico-chemical properties; nanosize; nanostructure; confinement and quantum-size effects

INTRODUCTION: THE WORLD OF OXIDE NANOMATERIALS

Metal oxides play a very important role in many areas of chemistry, physics and materials science.[1,2,3,4,5,6] The metal elements are able to form a large diversity of oxide compounds.[7] These can adopt a vast number of structural geometries with an electronic structure that can exhibit metallic, semiconductor or insulator character. In technological applications, oxides are used in the fabrication of microelectronic circuits, sensors, piezoelectric devices, fuel cells, coatings for the passivation of surfaces against corrosion, and as catalysts. In the emerging field of nanotechnology, a goal is to make nanostructures or nanoarrays with special properties with respect to those of bulk or single particle species.[8,9,10,11,12] Oxide nanoparticles can exhibit unique physical and chemical properties due to their limited size and a high density of corner or edge surface sites. Particle size is expected to influence three important groups of basic properties in any material. The first one comprises the structural characteristics, namely the lattice symmetry and cell parameters[13]. Bulk oxides are usually robust and stable systems with well-defined crystallographic structures. However, the growing importance of surface free energy and stress with decreasing particle size must be considered: changes in thermodynamic stability associate with size can induce modification of cell parameters and/or structural transformations[14,15,16] and in extreme cases the nanoparticle can disappear due to interactions with its surrounding environment and a high surface free energy.[17] In order to display mechanical or structural stability, a nanoparticle must have a low surface free energy. As a consequence of this requirement, phases that have a low stability in bulk materials can become very stable in nanostructures. This structural phenomenon has been detected in TiO_2, VO_x, Al_2O_3 or MoO_x oxides.[16,17,18]

Size-induced structural distortions associated with changes in cell parameters have been observed, for example, in nanoparticles of Al_2O_3,[17] NiO,[19] Fe_2O_3,[20] ZrO_2,[21] MoO_3,[23] CeO_2,[22] and Y_2O_3.[23] As the particle size decreases, the increasing number of surface and interface atoms generates stress/strain and concomitant structural perturbations.[24] Beyond this "intrinsic" strain, there may be also "extrinsic" strain associated with a particular synthesis method which may be partially relieved by annealing or calcination.[25] Also, non-stoichiometry is a common phenomenon.[25] On the other hand, interactions with the substrate on which the nanoparticles are supported can complicate the situation and induce structural perturbations or phases not seen for the bulk state of the oxide.[18,26]

The second important effect of size is related to the electronic properties of the oxide. In any material, the nanostruture produces the so-called quantum size or confinement effects which essentially arise from the presence of discrete, atom-like electronic states. From a solid-state point of view, these states can be considered as being a superposition of bulk-like states with a concomitant increase in oscillator strength.[27] Additional general electronic effects of quantum confinement experimentally probed on oxides are related to the energy shift of exciton levels and optical bandgap.[28,29] An important factor to consider when dealing with the electronic properties of a bulk oxide surface are the long-range effects of the Madelung field, which are not present or limited in a nanostructured oxide.[30,31,32] Theoretical studies for oxides show a redistribution of charge when going from large periodic structures to small clusters or aggregates which must be roughly considered to be relatively small for ionic solids while significantly larger for covalent ones.[33,34,35,36,37,38] The degree of ionicity or covalency in a metal-

oxygen bond can however strongly depend on size in systems with partial ionic or covalent character; an increase in the ionic component to the metal-oxygen bond in parallel to the size decreasing has been proposed.[15]

Structural and electronic properties obviously drive the physical and chemical properties of the solid, the third group of properties influenced by size in a simple classification. In their bulk state, many oxides have wide band gaps and a low reactivity.[39] A decrease in the average size of an oxide particle do in fact change the magnitude of the band gap,[32,40] with strong influence in the conductivity and chemical reactivity.[41,42] Surface properties are a somewhat particular group included in this subject due to their importance in chemistry. Solid-gas or solid-liquid chemical reactions can be mostly confined to the surface and/or sub-surface regions of the solid. As above mentioned, the two dimensional (2D) nature of surfaces has notable structural, typically a rearrangement or reconstruction of bulk geometries,[3,11,43] and electronic, e.g. presence of mid-gap states,[42,44] consequences. In the case of nanostructured oxides, surface properties are strongly modified with respect to 2D-infinite surfaces, producing solids with unprecedent sorption or acid/base characteristics.[45] Furthermore, the presence of under-coordinated atoms (like corners or edges) or O vacancies in an oxide nanoparticle should produce specific geometrical arrangements as well as occupied electronic states located above the valence band of the corresponding bulk material,[46,47,48] enhancing in this way the chemical activity of the system.[43,45,49,50]

In this Chapter we will analyze how nanoparticulated oxides are synthesized, their most significant physico-chemical properties, and will focus the ending part on several, well known oxides. Particular attention will be paid to the effect of the primary

nanostructure, e.g. primary particle size, on structural/electronic properties and how these alter other industrial-related properties.

SYNTHESIS OF NANOPARTICULATED OXIDES

The first requirement of any novel study of nanoparticulated oxides is the synthesis of the material. The development of systematic studies for the synthesis of oxide nanoparticles is a current challenge and, essentially, the corresponding preparation methods may be grouped in two main streams based upon the liquid-solid [51] and gas-solid[52] nature of the transformations.

Liquid-solid transformations are possibly the most broadly used in order to control morphological characterstics with certain "chemical" versatility and usually follow a "bottom-up" approach. A number of specific methods have been developed, among which those broadly in use are: ***1)*** Co-precipitation methods. This involves dissolving a salt precursor (chloride, nitrate, etc.) in water (or other solvent) to precipitate the oxo-hydroxide form with the help of a base. Very often, control of size and chemical homogeneity in the case of mixed-metal oxides are difficult to achieve. However, the use of surfactants, sonochemical methods, and high-gravity reactive precipitation appear as novel and viable alternatives to optimize the resulting solid morphological characteristics.[51,53,54] ***2)*** Sol-gel processing. The method prepares metal oxides via hydrolysis of precursors, usually alcoxides in alcoholic solution, resulting in the corresponding oxo-hydroxide. Condensation of molecules by giving off water leads to the formation of a network of the metal hydroxide: Hydroxyl-species undergo polymerization by condensation and form a dense porous gel. Appropriate drying and calcinations lead to

ultrafine porous oxides.[55] ***3)*** Microemulsion technique. Microemusion or direct/inverse micelles represent an approach based on the formation of micro/nano-reaction vessels under a ternary mixture containing water, a surfactant and oil. Metal precursors on water will proceed precipitation as oxo-hydroxides within the aqueous droplets, typically leading to monodispersed materials with size limited by the surfactant-hydroxide contact.[56] ***4)*** Solvothermal methods. In this case, metal complexes are decomposed thermically either by boiling in an inert atmosphere or using an autoclave with the help of pressure. A suitable surfactant agent is usually added to the reaction media to control particle size growth and limit agglomeration. ***5)*** Template/Surface derivatized methods. Template techniques are common to some of the previous mentioned methods and use two types of tools; soft-templates (surfactants) and hard-templates (porous solids as carbon or silica). Template- and surface-mediated nanoparticles precursors have been used to synthesize self-assembly systems. [51]

Gas-solid transformation methods with broad use in the context of ultrafine oxide powder synthesis are restricted to chemical vapor deposition (CVD) and pulsed laser deposition (PLD). ***6)*** There are a number of CVD processes used for the formation of nanoparticles among which we can highlight the classical (thermally activated/pydrolytic), metalorganic, plasma-assisted, and photo CVD methodologies.[57] The advantages of this methodology consist of producing uniform, pure and reproduce nanoparticles and films although requires a careful initial setting up of the experimental parameters. ***7)*** Multiple-pulsed laser deposition heats a target sample (4000 K) and leads to instantaneous evaporation, ionization, and decomposition, with subsequent mixing of desired atoms. The gaseous entities formed absorb radiation energy from subsequent

pulses and acquire kinetic energy perpendicularly to the target to be deposited in a substrate generally heated to allow crystalline growth.[58]

Irrespective of the preparation method use to obtain ultrafine nano-oxides, the studies of nanoparticle preparation yielded compelling evidence concerning the fact that crystallization does not follow a traditional nucleation and growth mechanism. Although subjected to further assessment, it appears that the simple idea that a small primary size would prime nucleation as the key step of crystallization seems essentially correct and holds certain general validity, at least in solid-solid crystallization mechanisms (e.g. heating of oxo-hydroxides to form oxides). When additional liquid/gas phase crystallization steps are involved in the final formation of the nanoparticle (e.g. as in solvothermal methods), other steps like Ostwald ripening may be also of prime importance. In any case, a lot of novel insights have been recently uncover in solid-solid transformations and two main theories describe crystallization to proceed either by surface (single particle) and/or interface (two or multiple particle) nucleation.[59,60] The primacy of one of them has been postulated to be a function of the oxide chemical nature and temperature, being presumably surface effects always predominant at higher temperatures. Both theories mostly received support from kinetic approaches but very recent analyses sensitive to structural order in the amorphous precursor materials have demonstrated the key role of intraparticle local order (below 1 nm) in driving the nucleation temperature onset in a broad interval of ca. 200 K, showing that the whole crystallization mechanism of oxide nanoparticles appears only compatible with some kind of intraparticle, dimensional-restricted ("surface") mechanism.[61] This invokes for the crucial structural characterization of the initial, XRD-amorphous materials in order to

further progress in the understanding the nanostructure influence in morphological properties of oxides.

PROPERTIES OF NANOPARTICULATED OXIDES

The current knowledge on oxide materials allows to affirm that most of their physico-chemical properties display an acute size dependence. Physico-chemical properties of special relevance in Chemistry are mostly related to the industrial use of oxides as sensors, ceramics, absorbents and/or catalysts. A bunch of novel application within these fields rely on the size-dependence of the optical, (electronic and/or ionic) transport, mechanical and, obviously, surface/chemical (redox, acid/base) properties of oxide nanomaterials. We should stress that size effects in oxide chemistry have frequently two interrelated faces, structural/electronic quantum-size and size-defect or non-stoichiometry effects. Hence, here we will describe the influence of these two phenomena in the main physico-chemical properties of oxides.

Optical properties. The optical conductivity is one of the fundamental properties of metal oxides and can be experimentally obtained from reflectivity and absorption measurements. While reflectivity is clearly size-dependent as scattering can display drastic changes when the oxide characteristic size (primary/secondary particle size) is in/out the range of photon wavelength,[62] absorption features typically command main absorption behavior of solids. Due to quantum-size confinement, absorption of light becomes both discrete-like and size-dependent. For nano-crystalline semiconductors, both linear (one exciton per particle) and non-linear optical (multiple excitons) properties arise as a result of transitions between electron and hole discrete or quantized electronic

levels. In the first case, depending on the relationship between the radius of the nano-particle (R) and the Bohr radius of the bulk exciton ($R_B = \varepsilon \hbar^2/\mu e^2$; μ exciton reduced mass and ε dielectric constant of the semiconductor), the quantum confinement effect can be divided into three regimes; weak, intermediate and strong confinement regimes, which correspond to $R >> R_B$, $R \approx R_B$, and $R << R_B$, respectively.[63] The effective mass theory (EMA) is the most elegant and general theory to explain the size dependence of the optical properties of nano-meter semiconductors, although other theories as the free-exciton collision model (FECM)[64] or those based in the bond length - strength correlation[65] have been developed to account for several deficiencies of the EMA theory.

For the onset of light absorption, e.g. the optical band gap, as well as for all other electronic transitions present in the optical absorption spectrum, the EMA theory predicts a r^{-2} dependence, with a main r^{-1} correction term in the strong confinement regime, while FECM gives a exp(1/r) behavior. It can be thus concluded that metal oxide semiconductors would present, as a first rough approximation, an optical band gap energy with an inverse squared dependence of the primary particle size if quantum confinement dominates the energy behavior of the band gap. Figure 1 shows that this happens to be the case for (direct band gap) Fe_2O_3[66] or (indirect band gap) CdO[67] but not for Cu_2O,[68] CeO_2,[69] ZnO,[70,71] and TiO_2.[72,73] Limited deviations from the R^{-2} behavior, as observed for ZnO[70] in Figure 1 or SnO_2,[74] can be based in the known fact that the theory overestimates the blue shift and can be justified with a proper calculation of electronic states by using simple quantum mechanical methods, while marked deviations are usually based in several chemical/physical phenomena not accounted for in the previous discussion. In the case of Cu_2O[68] or CeO_2,[75] it appears to be directly related with the presence of Cu^{2+}

(remarkably for very low particle size) and Ce^{3+} ions at the surface of the nanostructured materials. At the moment it is not clear if the presence of these oxidation states are intrinsic to the nanostructure or result from the specific procedure of preparation. The case of WO_3 share also some of the difficulties pointed out above. Kubo *et al.* were able to show that the band gap of this oxide decrease with size from ca. 3.0 to 2.8 eV as a function of R^{-1},[76] but the presence of a variable number of oxygen defects, reduced W redox states and mid-gap electronic states with size makes this an open question.[77] TiO_2 is the other example included in Fig. 1 having a band gap energy behavior with marked differences from that expected r^{-2} behavior. While bulk TiO_2 is an indirect semiconductor, nanostructured TiO_2 materials are likely direct ones.[72,78] This may be a general result. As discussed in ref. 79, the confinement of charge carriers in a limited space causes their wavefunctions to spread out in momentum space, in turn increasing the likehood of radiative transitions for bulk indirect semiconductors. This may also be the case of NiO.[80] The indirect nature of the absorption onset would complicate the analysis of the optical band gap energy due to the above mentioned step structure of the absorption onset (which includes phonon-related absorption/emission features).[81] In spite of this, the steady behavior shown in Fig. 1 can not be accounted for by small variations in the absorption onset and should be grounded in other physical phenomena.

Other optical excitations which showed quantum-size confinement effects concerns the excitation of optical phonons of oxides. The effects of size on the phonon spectra of oxide materials have been well established by using Raman scattering experiments on nanocrystals, in combination with the theoretical phonon confinement models.[-83] Essentially, the theoretical background for the study of nanocrystalline

materials is provided by the phonon confinement model. This factor is the main responsible for the changes observed in the Raman spectrum which are caused by the size effect. Nevertheless, other factors have been described which can contribute to Raman spectrum modification as the non-stoichiometry or the internal stress/surface tension. The phonon confinement model links q vector selection rule for the excitation of Raman active optical phonons with long-range order and crystallite size[82,83] In an amorphous material, owing to the lack of long-range order, the q-vector selection rule breaks down and the Raman spectrum resembles the phonon density of states. Nanocrystals represent an intermediate behavior. For a nanocrystal of average diameter L, the strict "infinite" crystal selection rule is replaced by a relaxed version, with the result that a range of q vectors is accessible due to the uncertainty principle.[84] The q vector relaxation model can be used for the purpose of comparing experimental data with theoretically predicted phonon confinement. According to this model, for finite sized crystals, the Raman intensity can be expressed using the equation 1:[82,85]

$$I(\omega) \cong \int_{BZ} \exp\left(-q^2 L^2 / 8\right) \frac{d^3 q}{\left[\omega - \omega(\vec{q})\right] + \left[\Gamma_0 / 2\right]^2} \qquad (1)$$

The $\rho(L)$ represents the particle size distribution, q is expressed in units of π/a_L (being a_L the unit cell parameter), $\omega(\vec{q})$ is the phonon dispersion, and Γ_0 is the intrinsic linewidth of the bulk crystal. A spherically symmetric phonon dispersion curve is assumed and approximated by a simple linear chain model.[84] For a given phonon mode, the slope of dispersion away from the BZ center determines the nature of the modification in the Raman line shape as a function of crystallite size: a negative slope, towards lower frequency, would produce a downshifted (red-shifted) Raman peak, while

a positive slope would result in an up-shifted (blue-shifted) Raman peak, in addition to an asymmetric peak broadening, as the crystallite size reduces. Usually is chosen for this kind of analysis the most intense Raman mode for the solid studied. Some examples of application of the confinement model for qualitative interpretation of Raman results in series of nanostructured oxides like anatase ZnO, TiO_2, CuO, Cr_2O_3, $ZrTiO_4$, CeO_2 or manganese oxides can be found elsewhere.[25,85,86,87,88,89,90,91,92]

In all cases, optical absorption features of nanosized oxides are additionally influenced by "non-stoichiometry" size-dependent defect effects. Typical point defects in nanostructured oxides concern oxygen or cation vacancies and/or the presence of aliens species, like Cu^{2+} and Ce^{3+}. Vacancy defects introduce gap states in proportion to the defect number; in fact, a random distribution of (equal) vacancy defects introduce a gaussian-like density of states which may produce mid-gap states and/or be localized near the valence and conduction bands depending on the electronic nature (donor/acceptor) of the defect and giving characteristic "localized" features in the UV-visible spectrum. Such point defects mainly contribute to the Raman spectra by producing a broadening of the peaks. Alien cations display specific features, like the localized d-d or f-f transitions of Cu/Ce. Besides electronic modifications, point defects but particularly alien ions, like Cu^{2+} and Ce^{3+} above, induce strain effects and concomitant structural differences in atomic positions with respect to bulk positions. The influence of strain in the optical absorption spectrum has been nicely demonstrated in the work of Ong et al. for ZnO,[93] showing the splitting of the first exciton peak for large values of compressive strain. Strain effects (including parameter variations measured in optical phonons with the help of the Gruneisen parameter) are inherent to nanostructured materials[25,71] and may be

comprised in the general, ambiguous term of "surface" effects usually claimed to account for significant deviations the confinement theories. Surface effects and, particularly, non-stoichiometry related to the preparation method are critically important for very low particle size and produce characteristic features in the UV-visible spectrum for certain oxides, as SnO_2[94] or ZrO_2.[95]

Transport properties. Oxide materials can present ionic or mixed ionic/electronic conductivity and it is experimentally well established than both can be influenced by the nanostructure of the solid. The number of electronic charge carriers in a metal oxide is a function of the band gap energy according to the Boltzmann statistics. The electronic conduction is referred to as n- or p-hopping-type depending on whether the principal charge carrier are, respectively, electrons or holes. The number of "free" electron/holes of an oxide can be enhanced by introducing non-stoichiometry and, in such case, are balanced by the much less mobile oxygen/cation vacancies. In an analogous manner to hoping-type conduction, ionic conduction takes place when ions can hop from site to site within a crystal lattice as a result of thermal activation, and is typically interpreted on the basis of a modified Fick´s second law. Four mechanism types have been observed for ionic conduction: direct interstitial, interstitialcy, vacancy, and grotthus. As charge species (defects; impurities) in polycrystalline oxides typically segregate to particle boundaries to minimize strain and electrostatic potential contributions to the total energy, there is a contribution to the conductivity parallel to the surface which becomes important at the nanoscale regime. The charge carrier (defect) distribution also suffers strong modification from bulk materials as there is presence of charge carries through the whole material as a consequence of the shielded electrostatic

potential depletion at surface layers of nanosized materials.[96] As a result of these nanoscale derived effects, it is well known that CeO_2 exhibits an improved n-type conductivity which may be four order of magnitude greater than the corresponding to bulk/micro-crystalline ceria, and is ascribed to a significant enhancement of the electronic contribution.[97] Alteration of the transport properties is also observed in ZrO_2 but the physical ground is still far from being understood.[96] The strong size-dependence observed for the electrical conductance in the context of gas-sensing devices has been recently reviewed for the SnO_2, WO_3, and In_2O_3 oxides.[98] In proton conductors, like $SrCe_{0.95}Yb_{0.05}O_{3-d}$, enhanced conduction and faster kinetics under H-atmospheres are observed in nanosized samples as these phenomena are largely determined by boundary/interfacial effects.[99] Interesting to stress here is that some of the most dramatic effects of he nanostructure on ionic transport in oxides are observed in the field of Li^+-ion batteries. An outstanding enhancement of Li^+-ion vacancy conductivity have been achieved using Li-infiltrated nanoporous Al_2O_3.[100]

Mechanical properties. Main mechanical properties concerns low (yield stress and hardness) and high (superpasticity) temperature observables. Information on oxide nanomaterials is scarce and mainly devoted to analyze sinterability, ductibility, and superpasticity. In particular, an important number of works have showed significant improvement in sintering with up to 600 K lower temperatures with respect to bluk counterparts. In conventional/bulk materials the yield stress (σ) and harness (H) follow the Hall-Petch (H-P) equation:

$$\sigma / H = \sigma_0 / H_0 + k\, d^{-1/2} \qquad (2)$$

where the initial constants describe friction stress and hardness, d is the primary particle/grain size and k the corresponding slope. The H-P effect in bulk materials is attributed to the particle/grain boundaries acting as efficient obstacles for slip transfer (stress) or dislocations (hardness). Typically by decrease the particle/grain size down to the order of a few tens nanometers the H-P slope, which is positive, gets smaller values. However, below such critical point it appears that conventional dislocation mechamisn(s) cease(s) to operate and a d^{-n} ($|n| > ½$) behavior or a "reversal" H-P mechanism would become progressively dominant.[101,102,103] On top of this, these mechanical properties are also found to be strain-rate dependent; an enhanced strain rate sensitivity at room temperature is observed for TiO_2 and ZrO_2 with decreasing primary particle/grain size. In spite of such facts, it is clear that oxide materials (like Al_2O_3, ZrO_2, CeO_2, and TiO_2) sintered under vacuum or using the spark plasma technique display enhanced yield strength and hardness with respect to conventional/bulk ceramic materials and have the additional properties of being transparent (films), being potential materials for the aerospatial industry.[102,103,104]

Superplasticity refers to the capacity of oxide materials to undergo extensive tensile deformation without necking or fracture. The phenomenological relationship for superplasticity is defined as:

$$\varepsilon = A\frac{DGb}{kT}\left(\frac{b}{d}\right)^{p}\left(\frac{\sigma}{G}\right)^{n} \qquad (3)$$

where ε is the strain rate, D is the adequate diffusion coefficient, G is the shear modulus, b is the Burger´s vector, σ is the applied yield strength, and p/n the particle size and yield strength exponents. Equation 3 implies that reduction of the particle size leads to an

increase of the superplasticity strain rate at constant temperature, or to a reduction in the superplasticity temperature as a constant strain rate, but very studies have been reported having oxides as the subject of the work. Essentially, policrystalline tetragonal ZrO_2 appears as the most celebrated example of a superpacticity ceramic, and together with TiO_2 are the only nano-oxides subjected to studies. At room temperature, nanocrystalline oxides may have a small amount of ductibility beyond that exhibited by bulk materials but they are not superplastics. Al high temperatures, they seem to exhibit significant compressive ductility and strain rate sensitivities that are indicate of superplasticity.[102]

Chemical properties. Metal oxides are used for both their redox and acid/base properties in the context of Absorption and Catalysis. The three key features essential for their application as absorbents or catalysts are (i) the coordination environment of surface atoms, (ii) the redox properties, and (iii) the oxidation state at surface layers. Both redox and acid/base properties are interrelated and may attempts can be found in the literature to establish correlations of both properties.[105,106] In a simple classification, oxides having only s or p electrons in their valence orbitals tend to be more effective for acid/base catalysis, while those having d or f outer electrons find a wider range of uses.

The solid in a given reaction conditions that undergoes reduction and reoxidation simultaneously by giving out surface lattice oxyen anions and taking oxygen from the gas phase is called a redox catalyst. This process necessarily demands microscopy reversibility and implies dynamic operation. The commonly accepted mechanism was developed by Mars van Krevelen and essentially implies that redox systems require high-electronic conduction cations to manage electrons and high oxygen-lattice mobility. Based on modern isotopic exchange experiments, the redox mechanism of chemical

reactions can be more specifically divided in (i) extrafacial oxygen in which adsorbed (oxygen) species react (electrophilic reaction), and (ii) interfacial oxygen where lattice oxygen vacancies are created (nucleophilic reaction). There are enormous evidence that nucleophilic oxygen is capable of carrying out selective oxidations while it seems that electrophilic species seems to exclusively work on non-selective ones. Latter, it was shown that hydrocarbon selective oxidation starts with H-abstraction steps and that the filling of oxygen vacancies require the cooperation of a significant number of cations.[105] So, typically, an oxidation reaction demands to optimize three important steps: the activation of the C-H bond and molecular oxygen, and the desorption of products (to limit over-oxidation). The effect of size on these key steps is unknown but can be speculated to be related to the oxidation state of surface cations and their ability to manage electrons and the influence of non-stoichiometry on the gas-phase oxygen species handling and activation.

Many oxides also display acid/base properties. Oxide materials can contain Bronsted and Lewis acid/base sites. Bronsted acid (A) and base (B) interactions consist of an the exchange of protons as $HA + B = A^- + HB^+$. Lewis proposed a different approach to measure acid-base interaction as depicted by $(B:) + A = {}^{d-}B \rightarrow B^{d+}$. Latter, Petterson introduced the concepts of hard and soft acid and base but, usually, acid/base properties of solid are rationalized in terms of Bronsted and Lewis definitions. In any solid, two independent variables, the acid/base strength and amount (density per surface unit) need to be addressed to give a complete picture of its acid/base characteristics. Such characteristics are basically linked to the nature (valence/cation size) of the element present in the oxide and general views of the behavior of Bronsted/Lewis acidity as a

function of solid state variables have been published.[106] Essentially, Lewis acidity is characeristic of ionic oxides and practically absent (unless very aggressive outgassing treatments) in covalent oxides. The strongest Lewis acid oxides are Al_2O_3 and Ga_2O_3. As a general rule, the stronger the Lewis acid, the few available sites (amount) due to the higher level of surface hydroxylation. As mentioned, because Lewis acidity is mostly associated to oxides with ionic character, Lewis basicity is mostly associated with them. This means that the stronger the Lewis acid sites, the weaker the basic sites and vice versa. On the contrary, most of the ionic metal oxides do not carry sufficiently strong Bronsted acidity to protonate pyridine or ammonia at room temperature although the more acid of them can do it at higher temperatures. In spite of this, the surface OH groups of most ionic oxides have a basic more than acid character. Covalent low-valent nonmetal oxides (SiO_2, GeO_x, BO_x) also show quite weak Bronsted acid properties. Finally, strong Bronsted acidity appears in oxides of elements with formal valence five or higher (WO_3, MoO_3, N_2O_5, V_2O_5, and S-containing oxides).

CASE STUDIES

Nanostructures have been prepared for many oxides but only in a few cases there are systematic reports concerning the nanostructure effect on the physical and/or chemical properties and behavior of the oxide materials. As most relevant case studies we will detail here the examples given by the Al_2O_3, MgO, ZrO_2, CeO_2, and TiO_2 oxide systems. In addition, we will briefly describe some sparse work devoted to other single oxide systems containing Zn Fe, and Sn. Much less is known for nanostructured mixed

oxides although a recent review on the catalytic use of solid solutions has been published.[107]

1.- Aluminium oxides. Attention in the Al-O system is centered in the Al_2O_3 stoichiometry due to its importance as a catalyst component or absorbent and ceramic material in a multitude of industrial processes. Novel nanostructured aluminas are currently used as a support of active phases in the field of catalysis or are coated with other materials, like YAG or nano-Ni/-W, to produce materials with unprecedent mechanical properties related to a strong resistance to deformation at moderates temperatures (YAG) or with hardness above 30 GPa (Ni,W).[5,96] There are seven Al_2O_3 polymorphs, although only four, called α, δ, θ, and γ, are typically involved in most of the indutrial processes.[108] Theoretical studies of $(Al_2O_3)_n$ ($n \leq 15$) small clusters yielded certain structural, electronic, and chemical (behavior against adsorbates) resemblances with some α-Al_2O_3 surfaces.[109] The γ-Al_2O_3 is the nanostructured phase commonly obtained by most synthetic methods but also the α-Al_2O_3 polymorph is synthesized having high surface area.[15] The corundum, α-Al_2O_3 structure is the bulk thermodymanically stable phase but the calorimetry work of McHale et al.[15] gives conclusive evidence that γ-Al_2O_3 has a lower surface energy and becomes energetically stable at size below a point close to 10 nm (surface BET area ca. 75 $m^2\ g^{-1}$). They also showed the importance of surface hydroxyls or water molecules in the energetics of surfaces.[15,110] The surface characteristics of the gamma phase were extensively studied by Knozinger and Ratnasamy,[111] and Busca complied the most recent work concerning the surface properties of the important (gamma, alpha, and others) alumina polymporhs.[106] In

addition, modern studies showed that surface chemistry of nanostructured alumina not only depends on primary particle size but also on nanoporosity characteristics.[112]

The gamma polymorph suffers a complex phase excursion in reaching the alpha phase by increasing the temperature; the delta alumina is typically observed between 973-1273 K, evolving in the theta phase which finally yields the alpha polymorph at temperatures between 1273-1373 K. The γ-δ-θ transformation occurs topotactically with extensive sintering and loss of surface area but maintaining the fcc cubic packing of the oxygen sub-lattice. This complex transformation has been theoretically adressed, confirming the simple idea that occurs through aluminium atom migration while oxygen atoms remains essentially fixed.[113] The number and nature of the intermediates as well as the temperature(s) of the γ to θ transformation depends on a wide number of parameters as the nature of the precursors or preparation pH[114] and, certainly, the initial size of the gamma phase.[115] The α phase is obtained by a nucleation growth mechanism by which the key step is the anion packing reordering from the cubic to a hexagonal structure.[15,114,115] The analysis of the θ → α phase transformation mechanism, whether is a shear mechanism with the shear in an oxygen lattice direction or is a diffusional one as a part of the typical "nucleation and growth" model mechanism, has been subjected to many studies.[116,117] Temperature of phase transformation to end into the alpha phase and presence of some of the mentioned intermediates phases not only depend on size but also on the presence of impurities as Si[118] or presence of surface stabilizers.[96] Doping is an obvious route to modify all the phase transformations mentioned, presumably by the initial occupation of some interstitial positions of the polymorphs, altering in this way the above mentioned cation movement paths[466] and being progressively at the surface layer

of grain boundaries of the material as the temperature increases. Typically, Ti and Mg do not alter the temperature of the phase transformation[119] while Y, Zr,[119] Er,[120] Ba, La and Pr[121] delay it and Fe,[122] Y and Cr[119] decrease it. As already noted for other oxides, the K, Ba, or La presence at the surface is also known to retard the phase transformation to alpha; the exact mechanism depends primarily on the hetero-atom concentration as above a certain limit the occurrence of binary phases is detected.[119,123] An alternative method to control the phase transformation temperature and alpha primary particle size involves the seeding of the starting material with well-controlled nanosized germs of the alpha polymorph.[119] Unfortunately, full details of the influence of all these variables in the phase behavior have not been addressed to date, although some attempts are reported.[115,116,117,119]

2.- MgO and other alkaline-earth oxides. Magnesium oxide (MgO) is widely used in the chemical industry as a scrubber for air pollutant gases (CO_2, NO_x, SO_x) and as a catalyst support.[124] It exhibits a rock salt structure like oxides of other alkaline earth metals. The non-polar (100) face is by far the most stable surface,[125,126,127] and particles of MgO usually display a cubic shape. For example, when Mg metal is burned in air or oxygen, the MgO smoke particles that are formed are almost perfect cubes having (100) faces.[128] Special procedures to prepare MgO nanoparticles exhibiting (110) and (111) faces have been partially successful,[129] but in general they tend to facet to surfaces containing (100) planes.[130] The rocksalt (110) surface is also non-polar, but its surface energy is twice that of a (100) surface. In the case of a (111) surface, the situation is more complex because it will contain either a layer of Mg cations or a layer of O anions. Neither of these planes is charge neutral (a net dipole moment exists).[124] Thus, MgO

nanoparticles exhibiting (111) faces are intrinsically unstable and should undergo a structural transformation.

Highly porous (~ 90%), high-surface area (~ 1000 m^2/g), thermally stable (1200 K) crystalline films of magnesium oxide nanostructures were prepared using a novel ballistic deposition technique (a collimated atomic beam of Mg was deposited on a silica support under a background pressure of O_2).[131,132] The films consisted of a tilted array of porous nanoscale crystalline filaments. Surprisingly, the individual filaments exhibited a high degree of crystallographic order with respect to each other.[131] The films had chemical binding sites analogous to those of MgO(100) surfaces.[131,132] However, the fraction of chemically active, high energy binding sites was greatly enhanced on the nanoporous film. Such properties make these materials attractive candidates for applications as sensors and heterogeneous catalysts.[131] For example, they display interesting chemical properties towards CO and n-alkanes[131,133]

In its bulk state, MgO is a highly ionic compound and a wide bandgap (~ 7 eV) insulator. For small nanoparticles of MgO, a reduction in the bandgap could be measured by using optical absorption techniques.[6,124] and the effects of the electrostatic Madelung potential could not be as strong as those in bulk MgO.[127] The Mg cations in a (100) face are pentacoordinated and have a charge that is close to that found for the cations in the bulk.[34] These atoms are expected to have a low activity[34] and may not be of interest in chemical applications of MgO nanoparticles. On the other hand, Mg atoms located at corner or edge sites of MgO nanoparticles have a relatively low coordination number and a positive charge that is substantially smaller than that in the bulk.[34,35] These cations are expected to be the chemically active sites of the nanoparticles.[134,135]

An important aspect to consider when dealing with MgO nanoparticles is the possible presence of O vacancies.[136] These can have a tremendous influence on the electronic and chemical properties of the nanoparticles. The anionic vacancies in MgO are known as F centers; depending on the charge one can have F, F^+, and F^{2+} centers which correspond to the removal of a neutral O atom, of an O^- or of an O^{2-} anion, respectively.[136] The F centers can be described as an electron pair trapped in the cavity left by the missing oxygen. They can produce electronic states localized well above the valence band of MgO.[137] The F^+ centers consist of a single electron associated with the vacancy and give rise to a typical signal in EPR.[138] Finally, F^{2+} centers are strongly electron deficient and have a tendency to ionize bonded molecules.[139] Theoretical studies have shown that the presence of O vacancies is essential for having MgO nanoparticles with high chemical activity.[34,136,139] In fact, the O vacancies are so reactive that they may not be stable under the chemical environment of most catalytic reactions.

For several industrial applications MgO is doped with small amounts of a transition metal.[124,125] Such doping can induce structural transformations and be used to stabilize MgO nanoparticles that expose (110) or (111) faces. The doping also can lead to perturbations in the electronic properties of the nanoparticles by favoring the formation of O vacancies or by introducing new occupied states above the valence band of MgO as shown in Figure **2**.[140] The position of the new occupied states depends on the nature of the dopant element. This phenomenon is particularly important when the doping is done with metals like Fe or Cr that induce states 2-3 eV above the MgO valence band. In general, the $TM_xMg_{1-x}O$ systems (TM= Ni, Fe, Mn, Cr) exhibit electronic and chemical properties different from those of pure MgO.[141,142,143,144,145,146]

Experimental and theoretical studies have been performed that allow to compare the chemical reactivity and surface properties of MgO nanoparticles, MgO bulk powders, and extended MgO(100) surfaces.[6,146,147] Thermal desorption spectra for CO on a MgO(100) single-crystal surface cleaved in vacuum exhibit a peak at ~ 60 K.[148] The adsorption energy on flat terraces of MgO is ~ 3.2 kcal/mol.[148] On defects or imperfections of MgO(100), the desorption temperature of CO can increase to ~ 120 K.[149] Cubic nanoparticles of MgO with a size larger than 150 nm (bulk-like systems) have a CO desorption temperature of ~ 135 K, while a CO desorption temperature of ~ 190 K is seen for MgO nanoparticles in the range of 4-6 nm.[6,147] This last temperature implies an increase of ~ 5 kcal/mol with respect to the CO adsorption energy on a perfect MgO(100) surface. Thus, the reactivity of the oxide systems increases following the sequence: MgO(100) surface < bulk-like MgO particles < MgO nanoparticles. An identical trend is found when comparing the corresponding NO desorption temperatures.[147] In the MgO nanoparticles one can expect a substantial percentage of Mg cations that have only four or three oxygen neighbors.[127] Theoretical studies have shown that these sites interact better with CO, NO, H_2O and SO_2 than the pentacoordinated Mg cations present in a perfect MgO(100) surface.[35,150,151] Water adsorbs and dissociates readily on small nanoparticles of MgO,[152,153] while no dissociation is seen on extended surfaces of bulk MgO. Bulk MgO is not useful for removing chlorine from chloroethylethyl sulfide (a mimic of mustard gas), whereas nanocrystals of MgO are highly reactive:[153]

$$2CH_3CH_2SCH_2CH_2Cl + MgO \rightarrow 2CH_3CH_2SCH{=}CH_2 + MgCl_2 + H_2O$$

These nanoparticles were generated by specially designed sol-gel or aerogel processes. [153] Depending on the exact procedure followed for the preparation, nanoparticles of MgO with polyhedral or hexagonal shapes can be synthesized, but they also contain OH groups. In these morphological shapes, the nanoparticles posses more defects than expected for the typical cubic shape of MgO.[153]

Cr-doped MgO systems adsorb CO stronger than pure MgO. Doping with Cr introduces occupied electronic states above the valence band of MgO (see Figure **2**) which are very efficient for bonding interactions with CO.[145,146] The adsorption energies of CO are ~ 15 and 19 kcal/mol on the $Mg_{0.93}Cr_{0.07}O(100)$ surface and $Mg_{0.95}Cr_{0.05}O$ nanoparticles (3-6 nm in size), respectively.[6] Again the nanoparticles bond CO better than the surface of the bulk oxide, probably due to the presence of corner or edge sites.[6,130]

Recently the preparation of nanoparticles of CaO and BaO is receiving a lot of attention due to their potential use in the control of NO_x emissions from automotive engines and the cleaning of other environmental pollutants. [153,154,155] As in the case of MgO, nanoparticles of CaO and BaO usually prefer to adopt a nearly perfect or somewhat distorted cubic shape, exposing the (100) face of a rocksalt crystal structure.[156,157] Nanoparticles exhibiting (110) and (111) faces are much less common and are not stable at high temperatures. In nanoparticles of CaO and BaO, the chemical activity is mainly associated with Ca, Ba or O atoms located at corner or edge positions in the cubic structure.[158,159]

3.- Ziconium oxides. Zirconium dioxide (ZrO_2) is very interesting from a technological point of view, since it can be used as a structural ceramic, a solid electrolyte, a gas sensor, and as a catalyst.[160,161,162,163,164] Decreasing the size of zirconia-based particles to

nanometric levels provides significant changes in their physical and chemical properties due to modifications produced at structural or electronic levels.[6] Pure bulk ZrO_2 exhibits three structures in different ranges of temperature at atmospheric pressure (other different orthogonal-type structures can be stabilized at high pressure).[165] The most stable thermodynamic form is monoclinic and transforms to unquenchable tetragonal and cubic (fluorite) structures at ca. 1400 and 2700 K (up to the melting point of ca. 2950 K), respectively.[165,166] A significant consequence of decreasing the size of pure zirconia is the possibility of stabilizing the tetragonal phase for particles of less than ca. 30 nm.[167] The characteristics of the tetragonal-monoclinic transition in the nanoparticles are affected by a number of intrinsic or extrinsic factors like the particle size, the pressure, potential mismatch between local and log-range order, or the presence of phase stabilizers either in the bulk (dopants) or at the surface (like water-derived or sulphate groups).[168,169,170,171,172,173,174,175] In general, it is agreed that the tetragonal-monoclinic transformation in nanosized pure zirconia is favored upon increasing the particle size or decreasing the pressure.[6]

As mentioned, stabilization of the tetragonal phase of zirconia can be achieved upon introduction of cationic dopants.[6,176,177,178] The amount of dopant required for the tetragonal stabilization in the nanoparticles generally depends on the nature of the dopant; a comparative study employing different rare-earth M^{3+} dopants shows that it decreases with increasing the ionic size of the dopant.[6,178] The nature of the dopant also affects the oxide ion conductivity in the nanoparticles, which, as observed for the extended systems,[177] increases with decreasing the ionic radius of the rare-earth dopant.[178]

The use of zirconia nanoparticles as starting material in the preparation of dense oxygen permeation membranes presents advantages since they exhibit improved sintering behavior[6,177,179] In addition, as pointed out for other oxide materials,[180] unique transport properties have been shown for membranes constituted by nanograins of stabilized zirconia.[181,182] Thus, in nanosized ytria-stabilized zirconia (YSZ), the activation energies of intragrain and grain boundary oxide ion conductivities were found to be slightly lower than in comparable microsize samples.[181]

Modification of the optical absorption properties upon decreasing particle sizes to sub-micrometric scale has also been observed.[6,95,183,184] An increase in the band gap energy observed for particles lower than 100 nm (0.25 eV shift upon decreasing the size to 1 nm) is well explained by quantum confinement effects except for particles lower than ca. 10 nm; deviations in such small size range are likely attributable to a crystalline → amorphous transition occurring for such very low size particles.[11,183] Another approach for modification of the optical properties of zirconia consists in surface modification of the nanocrystalline metal oxide particles with enediol ligands, resulting in red shifts of the optical absorption with respect to the unmodified nanocrystallite.[185] Such shifts are found to be proportional to the density of delocalised π electrons and the dipole moment of the surface oxide-ligand complex, decreasing with the ligand size. Coupling of this ligand-dependent (ligand to metal oxide) charge transfer interaction with the adjustable quantum size effects in the nanoparticles is interesting for tuning of electronic properties in frequency- selective photochemical applications.

4.- Cerium oxides. Ceria (CeO_2) is an oxide with important applications in areas of catalysis, electrochemistry, photochemistry and materials science.[186,187] In its most stable

phase, bulk CeO_2 adopts a fluorite-type Fm3m crystal structure in which each metal cation is surrounded by eight oxygen atoms.[187] The band gap of pure ceria is ~ 5 eV,[6] but crystal defects or impurities can transform the material in a good n-type semiconductor.[187] Experimental and theoretical studies indicate that bulk CeO_2 is not a fully ionic oxide.[188,189,190,191,192] CeO_2 is best described as an ionocovalent compound or covalent insulator.[190-192] One of the most interesting properties of ceria is its ability to undergo a facile conversion between "+4" and "+3" formal oxidation states.[166] Because of this, ceria is a key component in catalysts commonly used to reduce the emissions of CO, NO_x, and hydrocarbons from automobile exhaust,[193] or is used as base material of electrolytes and electrodes in solid oxide fuel cells.[186,187,194]

In the area of catalysis, nanoparticles of ceria have been studied since the early 1970s but they were poorly characterized.[194] In recent years, substantial progress has been made thanks the use of better synthetic methods and sophisticated techniques for characterizing structural and electronic properties.[195,196,197,198,199,200] It is not easy to find synthetic methods that allow the preparation of ceria nanoparticles that are small (< 3 nm) and have a narrow distribution of sizes.[6,103,194] However, it is known that very small particles of ceria may deviate from the fluorite structure of the bulk oxide.[6,103,201] For particles that are a little bit larger (4-7 nm), measurements of XAS, Raman and XRD would suggest the existence of local distortions on the cubic fluorite structure as a consequence of defects in the oxide lattice.[6,202,203] Depending on the method of preparation, and, particularly, of the Ce oxidation state of the precursor salt, the content of O vacancies and concomitant presence of Ce^{3+} in a ceria nanoparticle can change; this has been shown by using Raman and XRD.[6] Since "Ce^{3+}" is significantly bigger than

"Ce^{4+}" (atomic sizes 1.14 and 0.97 Å, respectively),[204] the presence of O vacancies increases the size of the unit cell and can distort it.[6,200] In addition to O vacancies, other structural imperfections as well as surface effects can be present in a ceria nanoparticle introducing strain in the lattice.[25,196,2001] Part of this strain can be removed by annealing at high temperatures, but sintering may concomitantly occur. Defects like dislocations, edges or cuts are probably removed during the sintering process. [6,200] The O vacancies and defects present in ceria nanoparticles can lead to special electronic properties, introducing electronic states within the band gap of the oxide. [6,194] Ceria particles with diameters of less than 10 nm have a substantially higher electronic conductivity than bulk ceria.[205]

Bulk ceria is able to absorb and store hydrogen.[206,207] Ceria nanoparticles have the same property.[200] The absorption of hydrogen causes an expansion in the lattice constant of the oxide detected by using XRD. Theoretical calculations indicate that the H atoms do not remain at a high-symmetry position in the center of the cavities of the ceria lattice, instead move towards the O sites forming hydroxyl species.[208] These species can be seen as the precursors for the removal of oxygen during a reduction process that generates Ce^{3+} cations. Results of temperature-programmed reduction and time-resolved XRD indicate that ceria nanoparticles reduce at temperatures that are lower than those seen for the reduction of bulk powders of ceria or well-defined CeO_2(111) surfaces.[208] During the reduction process, before the appearance of Ce_2O_3, there is a substantial expansion in the unit cell of the CeO_2 nanoparticles as a consequence of the embedding of hydrogen and the formation of O vacancies. The CeO_{2-x} nanoparticles adsorb CO and decompose NO and SO_2 at room temperature.

Ce-containing mixed-metal oxides. The performance of ceria in automotive catalysts and fuel cells can be enhanced by doping this oxide with a second metal (M= Zr, Ca, Cu, Au, Pt, Tb, La, Mn, etc).[209,210,211] Mixed-oxides maintain fluorite-type structures, particularly the cation sub-lattice, up to a high level of doping. The doping element in many cases enhances the thermal stability of the support system or favors the transport of oxygen (conversion between "Ce^{3+}" and "Ce^{4+}" oxidation states). In some situations, the doped-ceria nanoparticles become very active catalysts for reactions such as the water-gas shift or the destruction of SO_2.[194,208] This effect is achieved by doping with noble metals like Cu, Au or Pt, and the phenomenon is not fully understood.[212,213,214] However, as described below, these properties of ceria-based systems are mainly driven by two physico-chemical phenomena; the local M-O ordering and distance and the way the systems achieve charge neutrality, which in the case of ceria is mainly through presence of oxygen vacancies.

The CeO_2-ZrO_2 system is one of the most studied mixed-metal oxides in the literature due to its important role in the operation of automotive catalysts.[194] To enhance the redox properties and thermal stability of pure ceria, zirconia (ZrO_2) is often mixed as an additive to form solid solutions of the $Ce_{1-x}Zr_xO_2$ type ($x \approx 0.5$).[215,216,217] Typically, cations are randomly distributed in a cubic-type subcell, whereas the total symmetry is governed by the anion subcell. For these materials, several tetragonal (called t, t′, t′′) and cubic (c) structures are possible.[194] The presence of t′/t′′ metastable phases has been observed for Ce:Zr atomic ratios near to unity,[218] which are presumed to be stabilized by particle size (surface) effects in the nanometer regime (below ca. 15 nm).[219] In some cases, the mixed oxide lacks complete homogeneity, having microregions where the

content of Ce or Zr varies from the overall average composition, while in other it seems to have reasonable homogeneity.[220] Homogeneity at a local scale seems a crucial (although not unique) parameter to get improved thermal stability.[200,208] In general, the results of time-resolved XRD indicate that doping with Zr can enhance the thermal stability of ceria nanoparticles.[200]

In a recent study $Ce_{1-x}Zr_xO_2$ nanoparticles were found to be more reactive towards H_2 and SO_2 than $Ce_{1-x}Zr_xO_2(111)$ surfaces.[50] The $Ce_{1-x}Zr_xO_2(111)$ surfaces did not reduce in hydrogen at 300 ^oC. At temperatures above 250 ^oC, the $Ce_{1-x}Zr_xO_2$ nanoparticles reacted with H_2 and water evolved into gas phase with the generation of Ce^{3+} cations in the oxide matrix. [50] S K-edge XANES spectra pointed to SO_4 as the main product of the adsorption of SO_2 on the $Ce_{1-x}Zr_xO_2$ nanoparticles and $Ce_{1-x}Zr_xO_2(111)$ surfaces, see Figure **3**. Full dissociation of SO_2 was seen on the nanoparticles but not on the $Ce_{1-x}Zr_xO_2(111)$ surfaces.[50] The defects introduced by Zr into the ceria lattice favored the cleavage of the S-O bonds. [50]

One problem of Zr as a doping agent is the fact that it induces a very limited concentration of O vacancies in the ceria nanoparticles[208] and, thus, has a moderate effect on the redox properties of the system under oxidizing environment. To improve this aspect, one can try doping using Ca.[200,221] The introduction of Ca into a CeO_2-ZrO_2 oxidic network strongly modifies surface and bulk oxygen handling properties,[25,210,221] and CaO-CeO_2 catalysts are used for the destruction of SO_2.[221] The radii of atomic Ca (1.97 Å) and the "Ca^{+2}" cation (1.06 Å) are somewhat bigger than the corresponding radii of atomic Ce (1.83 Å) and the "Ce^{+4}" cation (0.97 Å).[222] According to formal oxidation states, a charge imbalance is produced in $Ce_{1-x}Ca_xO_2$ after replacing "Ce^{4+}" ions with

"Ca^{2+}" ions. In principle, this should induce the formation of O vacancies. However the situation is more complex, because the $Ce_{1-x}Ca_xO_2$ systems are far from being fully ionic.[200] Cation charges derived from DFT calculations indicate that these systems obey the Barr model[223,224] for charge redistribution in mixed-metal oxides. The Ca atoms in $Ce_{1-x}Ca_xO_2$ are more electropositive than the cations in CaO, while the Ce cations of $Ce_{1-x}Ca_xO_2$ are less electropositive than those of CeO_2.[200] These trends are consistent with XANES measurements at the Ca K- and Ce L_{III}-edges.[200] When taking a metal cation from a CaO matrix into a CeO_2 matrix, a gain in lattice strain occurs due to differences in metal-oxygen bond distances and in the number of oxygen neighbors per metal cation.[200] All these electronic and structural perturbations favor the creation of O vacancies. DFcalculations and molecular dynamics simulations indicate that the formation of O vacancies in $Ce_{0.75}Ca_{0.25}O_2$ is a much more exothermic reaction than the formation of O vacancies in CeO_2. Consistent with this prediction, the analysis of XRD data for $Ce_{0.8}Ca_{0.2}O_2$ and $Ce_{0.66}Ca_{0.33}O_2$ nanoparticles proves that their real compositions are $Ce_{0.8}Ca_{0.2}O_{1.82}$ and $Ce_{0.66}Ca_{0.33}O_{1.72}$, respectively.[200]

In a ceria lattice the presence of Ca (associated with O vacancies) introduces a larger strain than the presence of Zr. This phenomenon can be problematic at high temperatures.[25,200] For $Ce_{1-x}Ca_xO_{2-x}$ nanoparticles which contain a substantial amount of Ca ($x > 0.2$), experiments of time-resolved XRD show the segregation of CaO.[200] In technological applications at high temperature, one wants a dopant agent that introduces a reasonable amount of O vacancies in the lattice of ceria and produces a mixed-metal oxide that has a high thermal stability.[194] The compromise between these two properties depends on a significant number of variables. In any case, doping with Zr or Ca fully

satisfies only one of these two requirements. Doping simultaneously with Zr/Ca[25] or more simply with Tb and other lanthanides as Pr maybe a solution to this complex problem.[225] In the case of Tb, the relative stabilities of the "Tb^{3+}" and "Tb^{4+}" states favor the formation of O vacancies in $Ce_{1-x}Tb_xO_2$.[226] Thus, for a $Ce_{0.5}Tb_{0.5}O_2$ sample, the real composition is $Ce_{0.5}Tb_{0.5}O_{1.76}$. The O vacancies in the mixed-metal oxide make it chemically active towards H_2, NO, SO_2 and hydrocarbons.[50] A Rietveld analysis of XRD data for $Ce_{1-x}Tb_xO_2$ nanoparticles shows that terbium produces a small decrease in the lattice constant of the ceria host ($\leq$ 0.06 Å) and a relatively minor strain.[226] The $Ce_{1-x}Tb_xO_2$ nanoparticles do not exhibit phase segregation at elevated temperatures as the $Ce_{1-x}Ca_xO_2$ nanoparticles do. Studies comparing the thermal stability of CeO_2, $Ce_{0.66}Zr_{0.33}O_2$, $Ce_{0.66}Ca_{0.33}O_2$, and $Ce_{0.66}Tb_{0.33}O_2$ nanoparticles show sintering at temperatures above 600 ^oC.[6,226] The agglomeration rate increased following the order: $Ce_{0.66}Zr_{0.33}O_2 < Ce_{0.66}Tb_{0.33}O_2 < Ce_{0.66}Ca_{0.33}O_2 \approx$ nano ceria. This indicates that both Tb and Zr cations improve the thermal stability of the ceria nanoparticles, while Ca cations did not. For these samples, the magnitude of the strain at room temperature decreased according to the sequence: $Ce_{0.66}Ca_{0.33}O_2 > Ce_{0.66}Zr_{0.33}O_2 > Ce_{0.66}Tb_{0.33}O_2 >$ nano ceria.[226] Among the three types of doped ceria nanoparticles, the Tb-doped system had an intermediate thermal stability and concentration of O vacancies.[226] The combination of these two properties makes Tb-doped ceria nanoparticles special for applications in automotive catalysts.

$Ce_{1-x}Cu_xO_2$ nanoparticles are excellent precursors for water-gas shift catalysts.[227] The Cu atoms embedded in ceria had an oxidation state higher than those of the cations in Cu_2O or CuO.[228] The lattice of the $Ce_{1-x}Cu_xO_2$ systems still adopts a fluorite-type

structure, but has highly distorted with multiple cation-oxygen distances with respect to the single cation-oxygen bond distance seen in pure ceria.[227] The doping of CeO_2 with copper introduces a large strain into the oxide lattice and favors the formation of O vacancies. The $Ce_{1-x}Cu_xO_2$ nanoparticles are not stable under H_2 or CO atmospheres,[227,228] forming metallic Cu and partially reduced ceria. Interestingly, the reduction of the $Ce_{1-x}Cu_xO_2$ nanoparticles was completely reversible without the generation of CuO or Cu_2O phases during reoxidation.[228] This reversible process probably reflects the unusual structural and chemical properties of the $Ce_{1-x}Cu_xO_2$ nanomaterials.

5.- Titanium oxides. The Ti-O bond appears to have an increasing covalent character with the oxygen content of the oxide, so the departure of Ti^{n+} from formal oxidation state grows from +2 to +4.[229] Titanium dioxide (TiO_2) is one of the most prominent oxide materials for performing various kinds of industrial applications related to catalysis (among which the selective reduction of NOx in stationary sources,[230,231] and photocatalysis for pollutant elimination[232] or organic synthesis,[233] appear as rather important), its use as a white pigment in paintings,[234] as part of photovoltaic devices,[235] or electrochromic devices,[236] sensors,[237] as a food additive,[238] in cosmetics[239] and as a potential tool in cancer treatment.[240] In TiO_2 materials, the so-called "quantum-confinement" or "quantum-size effect" is restricted to very low sizes, below 10 nm, due to their rather low exciton Bohr radii. This would mean that a significant part of the potential novel chemical or physical applications needs to be carefully explored in the range of a few nanometers,.[6,241,242]

TiO_2 occurs in nature in three different polymorphs which, in order of abundance, are rutile, anatase, and brookite. Additional synthetic phases are called TiO_2(B), TiO_2(H) and TiO_2(R)[243] while several high pressure polymorphs have been also reported.[244] Mesoporuous amorphous materials have been additionally prepared having a Ti local structure similar to that present in surface/bulk nanostructured anatase samples.[245] As an extended (bulk) system, rutile is though to be the thermodynamic stable phase. When primary particle size is scaled down, a thermodynamic analysis of phase stability indicates that surface free energy and stress contributions stabilize anatase below a certain size close to 15 nm.[16] Above such limit, brookite and rutile appears to have very close free energy values up to a size close to 35 nm, above which rutile seems the stable phase.[16,246] First principles analysis of surface energy also suggests that the average surface energy of an anatase crystal may be lower than that of a rutile phase.[246] In contrast, experimental measurements of the surface stress contribution give, for a similar particle size, a larger value for the anatase than the rutile matrix.[247] In these nano-TiO_2 materials, surface energy appears to be related with the presence of under-coordinated Ti cations; the surfaces with fourfold-coordinated centers having larger energy than those with fivefold coordination, and the surface energy approximately increasing with the number of under-coordinated positions.[248] XAS measurements seem in agreement with this as only fivefold-coordinated Ti centers are observed at the surface of nanostructured materials,[249,250,251,252] although very small amorphous-like clusters (below 2 nm) may also present four-fold surface species.[253]

Although nanostructured anatase[254,255,256,257,258] rutile[255,256,257,,258,,259] and brookite[260,261] materials have been prepared, the above mentioned ideas suggest that a monphasic

nanoparticle with an average size in the 2-10 nm range is only possible with the anatase structure in absence of impurities (like Cl which may stabilize rutile, for example). Thus, upon heating, amorphous Ti-containing materials would transform on nanoparticulated anatase.[6,262] Exarhos et al. were the first to study the kinetics of the corresponding transition of amorphous films supported on silica substrates.[262] Under hydrothermal conditions, several groups gave evidence of the media influence (pH, presence of ions) on the crystallization mechanism and pointed out that the rate determining step can be related to the incorporation of new building units at the surface of the growing anatase crystal (solid-type step) and/or the dissolution of small anatase particles (Ostwald ripening; liquid-type step).[263,264,265,266] In other studies, using sol-gel[267,268] or microemulsion[59] procedures, details of the solid-state transformation mechanism leading to the anatase phase have been reported. Quantitative analysis of the key kinetic parameters controlling the amorphous titania to anatase transformation has been attempted in liquid media under hydrothermal conditions[262] and for solid-solid transformations concerning titania films,[262] powders,[59,268] or mesostructured[269] systems. The broad range of temperatures (623-873 K) where amorphous titania solids transform into anatase tells of a wide range of situations within the air-assisted transformation. In fact, crystallization has been considered to be controlled either by surface[59,262,267] or interface[268] nucleation processes. As a first approach, one may expect that interface nucleation can work at low temperature, starting from the lowest onset published (ca. 350 ^{o}C), while the surface dominated mechanism may get primacy above certain temperature, ca. 600 ^{o}C.[60] However, a point to stress is that all the above analyses are mainly of kinetic nature and always content several assumptions. So, recent approaches aimed to get rid of

such limitations and tried to establish the crystallization mechanism exclusively on structural basis.[61,270] From these studies and irrespective of the liquid- or gas-solid nature of the crystallization process, it was shown that precursor materials with may evolve either in anatase, rutile, and brookite display key differences in the amorphous intra-particle order, in particular, in the staking of sixfold-coordinated (TiO_6) and fivefold-coordinated (TiO_5) units. Although there are still unresolved issues, this interprets the physical basis of the crystallization and is only compatible with the dimensional-restricted (surface-type) nucleation mechanism.

The nanostructure of the TiO_2 material strongly affects the phase behavior, tuning the thermal stability and corresponding phase transformation of the polymorphs. Concerning anatase samples, the anatase → rutile phase transformation occurs in a broad temperature range, from around 723 to 1273 K.[59,60,271,272,273,274] As it is obvious, grain/particle size growth and phase transformation are parallel phenomena during a thermal treatment of a nanostructured solid but in TiO_2 the size-dependent relative stability of the polymorphs[16] interrelates these two variables, in turn difficulting the identification of themodynamic and kinetic parameters present in the phase transition. In ref. 271, it was shown that a smaller average primary particle size decreases the onset and the rate of the phase transformation, displaying thus a broader range of coexistence between anatase and rutile with decreasing particle size. Further analyses[272] indicate however that not only the primary but also the secondary particle size (e.g. the porosity of the sample) are key properties to modulate the anatase to rutile phase transformation. The exact influence of these variables is still a matter of debate. An even more complicated behavior is observed for brookite; the presence of anatase as an intermediate phase to a

final conversion into rutile also appears an up to date unveil function of the above mentioned variables.[16,271,272]

The nanostructure also affects other important properties of the TiO_2 material, of importance in its technological applications. As a semiconductor used in photochemical and photophysical applications, one critical parameter is the bangap energy and characteristics. Measurements of the optical bandgap give a variety of results; papers dedicated to optical measurements[6,80] give evidence of a steady behavior of the optical band gap energy as a function of primary particle size. In contrast, other works display the expected (based in a R^{-2} dependence of the optical band gap energy) blue shift of the exciton energy with decreasing particle size.[250] This apparent contradiction could be connected with the presence of impurities like carbon[275] and/or amorphous phases in the latter case, and thus be a consequence of the preparation method.

Electrical/ionic conductivity is the other type of property of the TiO_2 materials which can be modulate by nanostructure and finds current technological applications in the field of sensors or electronic devices. The metal/TiO_2 contact is used at low temperatures in sensor devices. At high temperatures, TiO_2 can be easily reduced and this decisively influences conductivity. The Titanium-oxygen phase diagram is very rich with many stable phases with a variety of crytal structures. As an example, the region TiO_2-Ti_2O_3 contents Ti_2O_3, Ti_3O_5, seven discrete phases of the homologous series Ti_nO_{2n-1} (Magnelli phases) and TiO_2.[276] Bulk defects result in n-type doping and high conductivity,[277] and are of various types like doubly charged oxygen vacancies, Ti^{3+}/Ti^{4+} interstitials, and planar defects like crystallographic shear planes,[277,278] while surface defects are mostly ascribed to under-coordinated Ti anions and (doubly charged) oxygen

vacancies.[16] Their presence, characteristics and development under reductive atmospheres as a function of temperature is less defined for nanostructured materials. Grain boundaries, on the other hand, strongly influence electrical conductivity as measured by impedance spectroscopy.[279] The onset temperature of the material reduction is expected to depend on defect nature and concentration and thus on primary particle size,[271,280] however this has not been fully analyzed in the literature.

Ti-containing mixed-metal oxides. The doping of TiO_2 structures constitutes an extensive field of research and requires a word apart. Surface and bulk doping have been used to stabilize the anatase or rutile phases, influence the temperature of the anatase → rutile phase transformation, modulate the optical band gap or alter the ionic/electrical conductivity by the presence of intrinsic vacancies. The properties of the mixed oxide depend primarily of the doping process nature; substitutional mixed oxides have been shown to be formed in the case of Ca, Sr, and Ba,[280] V,[249,281,282,283,284] Fe,[285,286] Cr,[282] Zr,[287,288] Ta,[285,289] Nb,[280,285,290] Mo,[291] W,[292,293,294] and Sn,[295,296] but in certain cases, like Cr or V, presence of interstitial cations are also observed as a function of the doping level and/or preparation method. Analysis of XRD/XAS/Neutron data indicate that the presence of anion vacancies for substitutional doping with trivalent/divalent ions and cation vacancies for W/Nb/Mo substitutional or V/Fe interstitial doping seems to be formed together with, for example, Ti lattice defects related to the presence of hydroxyls in the case of nanostructured Fe-doped TiO_2 calcined at $T < 673$ K,[285] or strong structural modifications in the oxygen sub-lattice in the case of nanostructured W-doped TiO_2.[293] Thus, charge neutrality appears to be a rather complex phenomena with elaborated structural/electronic implications both at local and long range order (forming thus

punctual and non-punctual defects), and with a more complex structural basis than, for example, the case of cerium oxide above detailed (previous subsection) On the other hand, the doping process typically decreases primary particle size when comparing with TiO_2 samples prepared in a similar way while the presence of hetero-atoms at the surface usually favors coalescence of grains/particles, with a concomitant increase of the secondary particle size and loss of surface area.[249,286,292] Concerning the influence in the phase stability and transformation, summaries of literature reports can be found in refs. 284, 289, and 297. These papers indicate that doping with Al, Ni, Ga, Nb, Ta, and W retards grain/particle growth of anatase and rutile phases and delays the anatase to rutile phase transformation while Mn, Fe, Cu and Zn generally promote the phase transformation. The theoretical basis of the different cation effect is however not known. It must be here recalled that such effect strongly depends, among other things, on the surface characteristics of the material and, therefore, of several phenomena like surface segregation or enrichment which are largely influenced by the preparation procedure; this limits the usefulness of the above generalization. Apart form that, the stable bulk phase is expected to have a lower solubility limit for dopants as it is "cation-rich" with respect to the stable nanostructured polymorph. This means that, for a total level of dopant, the degree of segregation at surface/grain boundaries will presumably increase as the primary size increases, limiting again the mentioned generalization. Other dopand atoms like Ca, Sr, and Ba,[281] or Sn[296] produce blue shifts of the optical band gap energy which may, at least, partially be due to a decrease in primary particle size and concomitant quantum confinement effect, likely associated to the presence of the hetero-atom in the TiO_2 structure. In the case of V, Cr, Nb, Mo, and W,[298] or rare earth atoms[299] a red shift of the

optical band gap appears to be observed. Appearance of hetero-metal states at the bottom of the conduction band seems a possible explanation for the band gap decrease. Some of these cations can additionally introduce detectable d-d transitions in the UV-vis spectra.[298,299]

6.- Other oxides. Nnostructured have been prepared for may oxides, but they have not been studied in a systematic way as described in previous sections. Some interesting cases will be discussed in this subsection. Here we will briefly describe some work devoted to other single oxide sysmtes containing Zn, Fe, and Sn.

Zinc oxide presents the wurtzite structure and dislays a high covalent Zn-O bond.[300] ZnO is a wide band gap semiconductor extensively studied due to its intrinsic properties but with a limited industrial use as a UV-blocker in sun lotions,[301] as a component in mixed oxide varistors,[302] as a catalyt/photcatalyst.[303] Additionaly, forthcoming applications are envisaged as a gas sensor,[98] solar cell and or/non-linear optical systems.[300,304] Of particular interest is the fact that ZnO can display novel nanostructures (nanorings, nanosprings, nanohelices, and nanobows), not typically observed in other oxides, due to the polar characteristics of their surfaces.[305] Surface and quantum size effects have been described as responsible of compressive strain and band gap blue shift in nanostructured ZnO nanoparticles.[70,93] However, surface effects and, particularly, non-stoichiomety and the presence of hydrogen (forming part ort no of hydroxyls) seem persistent phenomena with larger influence in the oxide properties when comparing with quantum-alone. Although acoustic phonons are dominated by quantum confinement,[306] optical phonons[25] and visible (yellow/green) luminescence[71] display properties mostly related to the presence of defects and/or hydrogen impurities without

significant chemical/physical sensibility to confinement. Chemical properties seems also enhanced by the nanostructure but again a critical role of oxygen vacancies and hydroxyl radicals is noticed.[303,307] There also been also a lot of work concerning ZnO-based mixed oxides mostly by doping with Mg, Mn, and Cd in order to modulate the band gap of the oxide.[308]

Fe and O form a number of phases, e.g., FeO (wustite); Fe_3O_4 (magnetite), α-Fe_2O_3 (hematite), γ-Fe_2O_3 (maghemite), and ε-Fe_2O_3.[309] The latter two phases are synthetic while remaining oxides occur in nature. The Fe-O phase diagram shows the predominance of the Fe_2O_3 stoichiometry for most temperature and pressure preparation conditions.[310] The magnetic properties of the Fe oxides have been extensively studied; in particular, the enhancing magnetic recording properties of magnetite[311] and maghemite[312] for nanostructured materials, or the use of the latter in Fe_2O_3-SiO_2 composite materials having magneto-optical properties.[313,314] Most physico-chemical studies are centered in the alpha (corundum structure with a distorted hexagonal anion closed-packed) and gamma (cubic inverse spinel) phases.[20,311,313,315,316,317] Size stability of the polymorphs has been studied but there is still a lack of consensus in a significant number of issues; particularly related to the existence of nano-particles with alpha structure.[20,317] As occurs with Ti-containing oxides, it appears that the presence of some anions, like Cl^-, strongly favors the production of a specific polymorph, α-Fe_2O_3,[316] while nitrate precursors yielded γ-Fe_2O_3[313,314,316] at low concentration of the precursor in the preparation solution but a mixture of these two phases at higher concentrations.[20] A significant difference between these two polymorphs comes from their surface structure as measured by XAS techniques. In the case of the alpha phase, Fe surface ions have a lowered local symmetry

(possibly fivefold coordinated) from the C_{3v} of the bulk,[315] while the gamma phase appears to have minimal modifications at the surface, in spite that two different local symmetries (O_h; T_d) can be encountered in such polymorph,[316] one of which would be likely favored at the surface. The γ-Fe_2O_3 converts to the alpha phase at rather low temperatures, above 623 K,[20,318,319] by a shear mechanism,[119] and the incorporation of gamma nanoparticles in polymeric, ceramic, or glassy matrices have been shown to stabilize the thermal evolution of the maghemite polymorph.[314,315] The influence of dopants has been also addressed in a few cases.[320] However, the influence of size, which is certainly presumed in the above mentioned stabilization mechanism, has not been fully addressed to date.

Tin (IV) oxide adopts the tetragonal rutile structure (cassiterite in its mineral form) with the (110) surface being the most stable one.[321,322,323,324] SnO_2 is a semiconductor with a direct but forbidden wide bandgap of ca. 3.6 eV.[325] The presence of oxygen deficiency in the nominally pure material induces n-type conductivity attributable to the appearance of shallow donor levels at ca. 0.03 and 0.15 eV below the conduction band.[326] Tin oxide is widely applied (in association with other metals in order to improve gas selectivity) as a sensor component, which is a consequence of the high sensitivity of its conductivity to the surrounding atmosphere. [98,327] Another application of SnO_2-based materials is in selective oxidation catalysis, in particular when combined with Sb.[328] Achievement of nanostructured configurations in the tin oxide particles is of high relevancy for both types of applications, in which the surface properties play a major role.[322,327,329] Thus, higher sensitivities and lower operation temperatures have been shown to be achieved upon lowering the particle size to the nanoscale in SnO_2-based

sensors.[98,326,330,] Such properties are closely related to strong variations of the surface electrical conductivity with deviation from stoichiometry.[326] In fact, non-stoichiometric surface layers of about 1 nm thick (with crystalline stoichiometric cores) are proposed to be present in SnO_2 nanoparticles from Raman results.[321] On the other hand, the variation observed in the electrical conductivity with oxygen pressure ($P^{-1/4}$ dependence) is compatible with singly ionized oxygen vacancies as the main structural defect in SnO_2 nanoparticles.[327]

Acknowledgements

Financial support from CICYT-SPAIN (projects CT2004-03409/BQU and CTQ2006-60480/BQU) and US Department of Energy (Division of Chemical Sciences; DE-AC02-98CH10886) is fully appreciated.

References

(1) Noguera, C. *Physics and Chemistry at Oxide Surfaces*; Cambridge University Press: Cambridge, UK, 1996.
(2) Kung, H.H. *Transition Metal Oxides: Surface Chemistry and Catalysis*; Elsevier: Amsterdam, 1989.
(3) Henrich, V.E.; Cox, P.A. *The Surface Chemistry of Metal Oxides*; Cambridge University Press: Cambridge, UK, 1994.
(4) Wells, A.F. *Structural Inorganic Chemistry, 6th ed*; Oxford University Press: New York, 1987.
(5) Rodríguez, J.A., Fernández-García, M; (Eds.) *Synthesis, Properties and Applications of Oxide Nanoparticles.* Whiley: New Jersey, 2007.
(6) Fernández-García, M.; Martínez-Arias, A.; Hanson, J.C.; Rodríguez, J.A. *Chem. Rev.* **2004**, *104*, 4063.
(7) Wyckoff, R.W.G. *Crystal Structures, 2nd ed*; Wiley: New York, 1964.
(8) Gleiter, H. *Nanostruct. Mater.* **1995**, *6*, 3.
(9) Valden, M.; Lai, X.; Goodman, D.W. *Science*, **1998**, *281*, 1647.
(10) Rodriguez, J.A.; Liu, G.; Jirsak, T.; Hrbek, Chang, Z.; Dvorak, J.; Maiti, A. *J. Am. Chem. Soc.* **2002**, *124*, 5247.

(11) Baumer, M.; Freund, H.-J. *Progress in Surf. Sci.* **1999**, *61*, 127.
(12) Trudeau, M.L.; Ying, J.Y *Nanostruct. Mater.* **1996**, *7*, 245.
(13) Ayyub, P.; Palkar, V.R.; Chattopadhyay, S.; Multani, M.; *Phys. Rev. B.* **1995**, *51*, 6135.
(14) (a) Millot, N.; Aymes, D.; Bernard, F.; Niepce, J.C.; Traverse, A.; Bouree, F.; Cheng, B.L.; Perriat, P. *J. Phys. Chem. B*, **2003**, *107*, 5740.(b) Schoiswohl, J.; Kresse, G.; Surnev, S.; Sock, M.; Ramsey, M.G.; Netzer, F.P. *Phys. Rev. Lett.* **2004**, *92*, 206103.
(15) McHale, J.M.; Auroux, A.; Perrota, A.J.; Navrotsky, A.; *Science* **1997**, *277*, 788.
(16) Zhang, H.; Bandfield, J.F.; *J. Mater. Chem.* **1998**, *8*, 2073.
(17) Samsonov, V.M.; Sdobnyakov, N.Yu.; Bazulev, A.N. *Surf. Sci.* **2003**, *532-535*, 526.
(18) Song, Z.; Cai, T.; Chang, Z.; Liu, G.; Rodriguez, J.A.; Hrbek, J. *J. Am. Chem. Soc.* **2003**, *125*, 8060.
(19) Rodriguez, J.A.; Rodriguez, L.; Ruette, F.; Gonzalez, L. in preparation.
(20) Ayyub, P.; Multani, M.; Barma, M.; Palkar, V.R.; Vijayaraghavan, R. *J. Phys. C: Solid State Phys.* **1988**, *21*, 229.
(21) Garvie, R.C.; Goss, M.F. *J. Mater. Sci.* **1986,** *21*, 1253.
(22) Hernández-Alonso, M.D.; Hungría, A.B.; Coronado, J.M.; Martínez-Arias, A.; Conesa, J.C.; Soria, J.; Fernández-García, M.; *Phys. Chem. Chem. Phys.* **2004**, *6*, 3524.
(23) Skandan, G.; et al. *Nanostruct. Mater.* **1992**, *1*, 313.
(24) Cammarata, R.C.; Sieradki, K.; *Phys. Rev. Lett.* **1989**, *62*, 2005.
(25) (a) Fernandez-Garcia, M., Wang, X.; Belver, C; Hanson, Iglesias-Juez, A.; J.C.; Rodriguez, J.A.; *Chem. Mater.* **2005**, *17*, 4181; (b) Alim, K.A.; Fonobevor, V.A.; Balandin, A.A.; *Appl. Phys. Lett.* **2005**, *86*, 053103.
(26) Surnev, S.; Kresse, G.; Ramsey, M.G.; Netzer, F.P. *Phys. Rev. Lett.* **2001**, *87*, 86102.
(27) Moriarty; P.; *Rep. Prog. Phys.* **2001**, *64*, 297.
(28) Yoffre, A.D.; *Advances in Physics* **1993**, *42*, 173.
(29) Brus, L.; *J. Phys. Chem.* **1986**, *90*, 2555.
(30) Pacchioni, G.; Ferrari, A.M.; Bagus, P.S. *Surf. Sci.* **1996**, *350*, 159.
(31) Mejias, J.A.; Marquez, A.M.; Fernandez-Sanz, J.; Fernandez-Garcia, M.; Ricart, J.M.; Sousa, C.; Illas, F. *Surf. Sci.* **1995**, *327*, 59.
(32) Fernández-García, M.; Conesa, J.C.; Illas, F.; *Surf. Sci.* **1996**, *349*, 207.
(33) Albaret, T.; Finocchi, F.; Noguera, C. *Faraday Discuss.* **2000**, *114*, 285.
(34) Rodriguez, J.A.; Maiti, A. *J. Phys. Chem. B*, **2000**, *104*, 3630.
(35) Rodriguez, J.A.; Jirsak, T.; Chaturvedi, S. *J. Chem. Phys.* **1999**, *111*, 8077.
(36) Bredow, T.; Apra, E.; Catti, M.; Pacchioni, G. *Surf. Sci.* **1998**, *418*, 150.
(37) Casarin, M.; Maccato, C.; Vittadini, A. *Surf. Sci.* **1997**, *377-379*, 587.
(38) Scamehorn, C.A.; Harrison, N.M.; McCarthy, M.I. *J. Chem. Phys.* **1994**, *101*, 1547.
(39) Rodriguez, J.A. *Theor. Chem. Acc.* **2002**, *107*, 117.
(40) Rodriguez, J.A.; Chaturvedi, S.; Kuhn, M.; Hrbek, J. *J. Phys. Chem. B*, **1998**, *102*, 5511.
(41) Hoffmann, R. *Solids and Surfaces: A Chemist's View of Bonding in Extended Structures*; VCH: New York, 1988.
(42) Albright, T.A.; Burdett, J.K.; Whangbo, M.H. *Orbital Interactions in Chemistry*; Wiley-Interscience: New York, 1985.
(43) Luth, H.; *Surface and interface of solid materials*; Springer, Berlin, 1997.

(44) Bardeen, J.; *Phys. Rev.* **1947**, *71*, 717.
(45) Jeevanadam, J.; Klabunde, K.J.; *Adsorbents* in "Synthesis, Properties and Applications of Oxide Nanoparticles" (Rodríguez, J.A., Fernández-García, M; Eds.). Whiley: N.J., 2007. Chpt. 14.
(46) Anchell, J.L.; Hess, A.C. *J. Phys. Chem.* **1996**, *100*, 18317.
(47) Rodriguez, J.A.; Hrbek, J.; Dvorak, J.; Jirsak, T.; Maiti, A. *Chem. Phys. Lett.* **2001**, *336*, 377.
(48) Ferrari, A.M.; Pacchioni, G. *J. Phys. Chem.* **1995**, *99*, 17010.
(49) Richards, R., Li, W.; Decker, S.; Davidson, C.; Koper, O.; Zaikovski, V.; Volodin, A.; Rieker, T.; *J. Am. Chem. Soc.* **2000**, *122*, 4921.
(50) Rodriguez, J.A.; Wang, X.; Liu, G.; Hanson, J.C.; Hrbek, J.; Peden, C.H.F.; Iglesias-Juez, A.; Fernández-García, M. *J. Molec. Catal. A: Chemical* **2005**, *228*, 11.
(51) D´Souza; L.; Richards, R.; *Synthesis of Metal-Oxide Nanoparticles: Liquid-Solid transformations* in "Synthesis, Properties and Applications of Oxide Nanoparticles" (Rodríguez, J.A., Fernández-García, M; Eds.). Whiley: N. J., 2007. Chpt. 3.
(52) Buzby; S.; Franklin, Rs.; Shah, S.I.; *Synthesis of Metal-Oxide Nanoparticles: Liquid-Solid transformations* in "Synthesis, Properties and Applications of Oxide Nanoparticles" (Rodríguez, J.A., Fernández-García, M; Eds.). Whiley: N.J., 2007. Chpt. 4.
(53) Suslick, K.S.; Choe, S.B.; Cichowlas, A.A.; Geenstaff, M.W.; *Nature* **1991**, *353*, 414.
(54) Chen, J.-F.; Wang, Y.-H.; Gou, F.; Wang, X.-M.; Zheng, C.; *Ind. Eng. Chem. Res.* **2002**, *39*, 948.
(55) Interrante, L.V.; Hampen-Smith, M.J.; *Chemistry of Advanced Materials: An Overview*, While-VCH: New York, 1998.
(56) Uskokovick, V.; Drofenik, M.; *Surf. Rev. Letter* **2005**, *12*, 239.
(57) Ohring, J. *The Material Science of Thin Films*. Academic-Press: San Diego, 1992.
(58) Hubler, G.K.; *Mater. Res. Bull.* **1992**, *17*, 25.
(59) Fernandez-Garcia, M., Wang, X.; Belver, C; Hanson, J.C.; Rodriguez, J.A.; *J. Phys. Chem. C* **2007** *111*, 674.
(60) Zhang, H.; Bandfield, J.F.; *J. Phys. Chem. C* **2007**, *111*, 6621.
(61) Fernandez-Garcia, M., Belver, C; Wang, X.; Hanson, J.C.; Rodriguez, J.A.; *J. Am. Chem. Soc.* **2007** (in press).
(62) Scott, B.J.; Wirnsberger, G.; Stocky, G.D.; *Chem. Mater.* **2001**, *13*, 3140.
(63) Yoffre I, *Adv. Phys.* 50, 1 (2001).
(64) Glinka YD, Lin SH, Hwang LP, Chen YT, Tolk NH, *Phys. Rev. B* **2001**, *64*, 085421.
(65) Pan LK, Sun CQ, *J. Appl. Phys.* **2004,** *95*, 3819.
(66) Iwamoto, M.; Abe, T.; Tachibana, Y.; *J. Mol. Catal. A* **2000,** *55*, 143.
(67) Vigil, O.; Cruz, F.; Morales-Acabedo, A.; Contreras-Puente, G.; Vaillant, L.; Santana, G.; *Mat. Chem. Phys.* **2001,** *68*, 249.
(68) Borgohain, K.; Morase, N.; Mahumani, S.; *J. Appl. Phys.* **2002,** *92*, 1292.
(69) Suzuki, T.; Kosacki, I.; Petrovsky, V.; Anderson, H.U.; *J. Appl. Phys.* **2001,** *91*, 2308.
(70) Viswanaha, R.; Sapra, S.; Satyani, B.; Der, B.N.; Sarma, D.D.; *J. Mat. Sci.* **2004**, *14*, 661.

(71) Li, L.; Qui ,X.; Li, G.; *J. Appl. Phys.* **2005,** *87*, 124101.
(72) Serpone, N.; Lawless, D.; Khairutdinov, R.; *J. Phys. Chem.* **1995**, *98*, 16646.
(73) Monticone, S.; Tufeu, R.; Kanaev, A.V.; Scolan, E.; Sánchez, C.; *Appl. Surf. Sci.* **2000,** *162-163*, 565.
(74) Deng H, Hossenlopp JM, *J. Phys. Chem. B* **2005**, *109*, 66.
(75) Tsunekawa, S.; Fukuda, T.; Kasuya, A.; *J. Appl. Phys.* **2000**, *87*, 1318.
(76) Kubo T, Nishikitani Y, *J. Electrochem. Soc.* **1998**, *145*, 1729.
(77) Karazhanov SZh, Zhang Y, Wang L-W, Masacarenas A, Deb S, *Phys. Rev. B* **2003**, *68*, 233204.
(78) Reddy, K.M.; Manorama, S.V.; Reddy, A.R.; *Mater. Chem. Phys.* **2002**, *78*, 239.
(79) Iyer, S.S.; Xie, Y.-H.; *Science* **1993**, *260*, 40.
(80) Mahmond, S.A.; Akl, A.A.; Kand, H.; Adbel-Had, K.; *Physica B* **2002,** *111*, 366.
(81) Matsumoto, T.; Suzuki, J.-I.; Ohmura, M.; Kanemitsu, Y.; Masumoto Y.; *Phys. Rev. B* **2001**, *63*, 195322.
(82) Richter H, Wang ZP, Ley L, *Solid State Commun.* **1981,** *39*, 625.
(83) Doss CJ, Zallen R, *Phys. Rev. B* **1993**, *21*, 15626.
(84) Nelly S, Pollak FH, Tomkiewicz M, *J. Phys. Chem. B* **1997**, *101*, 2730.
(85) Zhang, W.F.; He, Y.L.; Zhang, M.S.; Yin, Z.; Chen, Q. *J. Phys. D: Appl. Phys.* **2000**, *33*, 912.
(86) Swamy, V.; Muddle, B.C.; Dai, Q.; *Appl. Phys. Lett.* **2006**, *89*, 163118.
(87) Xu, J.F.; Ji, W.; Shen, Z.X.; Li, W.S.; Tang, S.H.; Ye, X.R.; Jia, D.Z.; Xin, X.Q. *J. Raman Spect.* **1999**, *30*, 413.
(88) Zuo, J.; Xu, C.; Hou, B.; Wang, C.; Xie, Y.; Qian, Y. *J. Raman. Spectrosc.* **1996**, *27*, 921.
(89) Zuo, J.; Xu, C.; Liu, Y.; Qian, Y. *Nanost. Mater.* **1998**, *10*, 1331.
(90) Kim, Y.K.; Jang, H.M. *Solid. State Commun.* **2003**, *127*, 433.
(91) Zhen, Z.; Tan, S.; Zhang, S.; Wang, J.; Jin, S.; Zhang, Y.; Sekine, H. *Jpn. J. Appl. Phys.* **2000**, *39*, 6293.
92 Popovic, Z.V.; Dohcevic-Mitrovic, Z.; Konstantinovic, M.J.; Scepanovic, M.; *J. Raman. Specrosct.* **2007**, *38*, 750.
(93) Ong, H.C.; Zhu, A.X.E.; Du, G.T.; Appl. Phys. Lett. **2002** *80*, 941.
(94) Kang, J.; Tsunekawa, S.; Kasuya, A.; Appl. Surf. Sci. **2001**, *174*, 306.
(95) Chang, S-M.; Doong, R-A.; *Chem. Mater*. **2007,** *19*, 4108..
(96) Mather, G.C.; Martinez-Arias; A.; *Transport properties and Oxygen Handling* in "Synthesis, Properties and Applications of Oxide Nanoparticles" (Rodríguez, J.A., Fernández-García, M; Eds.). Whiley: N.J., 2007. Chpt. 13.
(97) Chiang, Y.-M.; Lavik, E.B.; Kosacki, I.; Tuller, H.L.; Ying, J.H.; *J. Electroceram.* **1997**, *1*, 7.
(98) Franke M.E.; Koplin, T.J.; Simon, U.; *Small* **2006**, *2*, 36.
(99) Kosacki, I, Anderson, H.U.; *Solid State Ionics* **1997**, *97*, 429.
(100) Maekawa, H.; Tanaka, R.; Sato, T.; Fujimaki, Y.; Yamamura, T.; *Solid State Ionics* **2004**, *175*, 281.
(101) Weertman, J.R.; Averback, R.S. *Mechanical properties* in "Nanomaterials: synthesis, properties and applications" (Edelstein, A.S.; Cammarata, R.C.; Eds.). Inst. Physics Publishing: London, 1996.

(102) Tjong, S.C.; Chen, H.; *Mat. Sci. Eng.* **2004**, *45*, 1.
(103) Zhang, Z.; Seal, S.; Patil, S.; Zha, C.; Xue, Q.; *J. Phys. Chem. C.* **2007**, *111*, 11756.
(104) Lu, L.; Li, S.X.; Lu, K.; *Scr. Mater.* **2001**, *45*, 1163.
(105) Reddy, B.M.; *Redox properties of oxides* in "Metal Oxides" (Fierro, J.L.G:; Ed.). CRC, Boca Ratón, 2006.
(106)Busca, G.; *The surface acidity and basicity of solid oxides and zeolites* in "Metal Oxides" (Fierro, J.L.G:; Ed.). CRC, Boca Ratón, 2006.
(107) Cimino, A.; Stone, F.S.; *Adv. Catal.*, **2002**, *47*, 141.
(108) Stumpf, H.C.; Russel, A.S.; Newsome, J.W.; Tucker, C.M.; *Ind. Eng. Chem.*, **1950**, *42*, 1398.
(109) Fernández, E.M.; Eglitis, R.; Borstel, G.; Balbás, L.C.; *Phys. Stat. Sol. B* **2005**, *242*, 807; and references therein.
(110) McHale, J.M.; Novrotsky, A.; Perrota, A.J.; *J. Phys. Chem. B*, **1997**, *102*, 603.
(111) Knozinger, H.; Ratnasamy, P.; *Catl. Rev. Sic. Eng.*, **1978**, *17*, 31.
(112) Wang, Y.; Bryan, C.; Xu, H.; Pohl, P.; Yang, Y.; Brinker, C.J.; *J. Colloid Interf. Sci.* **2002**, *254*, 23.
(113) Cai, S.-H.; Rashkeev, S.N.; Pantelides, S.T.; Sohlberg, K.; *Phys. Rev. B* **2003**, *67*, 224104.
(114) Sharma, P.K.; Varadan, V.V.; Varadan, V.K.; *J. European Ceramic Soc.* **2003**, *23*, 659.
(115) Noda, H.; Muramoto, H.K.; *J. Mater. Sci.* **2003**, *38*, 2043.
(116) Bagwell, R.B.; Messing, G.L.; Howell, P.R.; *J. Mater. Sci.* **2001**, *36*, 1833.
(117) Yen, F.S.; Wen, H.L.; How, Y.T.; *J. Crys. Growth* **2001**, *233*, 761.
(118) McHale, J.M.; Yureki, K.; Dabbs, D.M.; Novrotsky, A.; Sunderesan, S.; Aksay, I.A.; *Chem. Mater.*, **1997**, *9*, 3096.
(119) Bowen, P.; Carry, C.; *Powder Technol.* **2002**, *128*, 248.
(120) Ragan, D.D.; Mates, T.; David, R.; *J. American Ceramics Soc.* **2003**, *86*, 541.
(121) Rossignol, S.; Kappenstein, C.; *Int. J. Inorg. Mat.* **2001**, *3*, 51.
(122) Appel, S.; Clausen, R.; Chouvankov, A.; Natter, H.; Hempelman, R.; Sabine, X.; Vollath, D.; *Ceramic Eng. Sci. Proceedings* **2002**, *23*, 585
(123) Zou, H.; Ge, X.; Shen, J.; *Thermochim. Acta* **2003**, *397*, 81.
(124) Föller, A.M. *Magnesium Oxide and its Applications*; Vollhardt: Berlin, 1978.
(125) Tasker, P.W. *Adv.* in *Ceramics,* **1984**, *10*, 176.
(126) Gibson, A.; Haydock, R.; LaFemina, J.P. *J. Vac. Sci. Technol. A* **1992**, *10*, 2361.
(127) Stener, M.; Fronzoni, G.; De Francesco, R. *Chem. Phys.* **2005***, 309*, 49.
(128) Moodie, A.F.; Warble, C.E. *J. Crystal Growth*, **1971**, *10*, 26.
(129) Mackrodt, W.C.; Tasker, P.W. *Chem. Britain*, **1985**, *21*, 13.
(130) DeSantis, E.; Ferrari, J. private communication.
(131) Dohnálek, Z.; Kimmel, G.A.; McCready, D.E.; Young, J.S.; Dohnálková, A.; Smith, R.S.; Kay, B.D. *J. Phys. Chem. B*, **2002**, *106*, 3526.
(132) Kim, J.; Dohnalek, Z.; White, J.M.; Kay, B.D. *J. Phys. Chem. B,* **2004**, *108*, 11666.
(133) Tait, S.L.; Dohnalek, Z.; Campbell, C.T.; Kay, B.D. *J. Chem. Phys.* **2005**, *122*, 164708.
(134) Rodriguez, J.A.; Jirsak, T.; Kim, J.-Y.; Larese, J.Z.; Maiti, A. *Chem. Phys. Lett.* **2000**, *330*, 475.

(135) Soave, R.; Pacchioni, G. *Chem. Phys. Lett.* **2000**, *320*, 345.
(136) Pacchioni, G.; Pescarmona, P. *Surf. Sci.* **1998**, *412/413*, 657.
(137) Gibson, A.; Haydock, R.; LaFemina, J.P. *Appl. Surf. Sci.* **1993**, *72*, 285.
(138) Giamello, E.; Paganini, M.C.; Murphy, D.M.; Ferrari, A.M.; Pacchioni, G. *J. Phys. Chem.* **1997**, *101*, 971.
(139) Ferrari, A.M.; Pacchioni, G. *J. Phys. Chem.* **1996**, *100*, 9032.
(140) Rodriguez, J.A. *Catal. Today* **2003**, *85*, 177.
(141) Rodriguez, J.A.; Jirsak, T.; Pérez, M.; Chaturvedi, S.; Kuhn, M.; González, L.; Maiti, A. *J. Am. Chem. Soc.* **2000**, *122*, 12362.
(142) Nagaoka, K.; Karasuda, T.; Aika, K. *J. Catal.* **1999**, *181*, 160.
(143) Rodriguez, J.A.; Jirsak, T.; Pérez, M.; González, L.; Maiti, A. *J. Chem. Phys.* **2001**, *114*, 4186.
(144) Tomishige, K.; Chen, Y.; Fujimoto, K. *J. Catal.* **1999**, *181,* 91.
(145) Rodriguez, J.A.; Jirsak, T.; Freitag, A.; Larese, J.Z.; Maiti, A. *J. Phys. Chem. B*, **2001**, *104*, 7439.
(146) Rodriguez, J.A.; Jirsak, T.; González, L.; Evans, J.; Perez, M.; Maiti, A. *J. Chem. Phys.* **2001**, *115*, 10914.
(147) DeSantis, E.; Ferrari, J.; González, L.; Pérez, M.; Evans, J.; Rodriguez, J.A. to be published.
(148) Wichtendahl, R.; Rodriguez-Rodrigo, M.; Härtel, U.; Kuhlenbeck, H.; Freund, H.-J. *Phys. Status Solidi A*, **1999**, *173*, 93.
(149) He, J.-W.; Estrada, C.A.; Corneille, J.S.; Wu, M.-C.; Goodman, D.W. *Surf. Sci.* **1992**, *261*, 164.
(150) Pacchioni, G. *Surf. Rev. Lett.* **2000**, *7*, 2777.
(151) Pacchioni, G.; Clotet, A.; Ricart, J.M. *Surf. Sci.* **1994**, *315*, 337.
(152) McGraw, L.T.; Yu, C.-M.; Thomas, J. *Langmuir*, **2000**, *23*, 352.
(153) Klabunde, K.J.; Stark, J.; Koper, O.; Mobs, C.; Park, D.G.; Decker, S.; Jiang, Y.; Lagadic, I.; Zhang, D. *J. Phys. Chem.* **1996**, *100*, 12142.
(154) Schmitz, P.J.; Baird, R.J. *J. Phys. Chem. B*, **2002**, *106*, 4172.
(155) Wang, X.; Hanson, J.; Rodriguez, J.A.; Szanyi, J., in preparation.
(156) Carnes, C.L.; Klabunde, K.J.; *Chem. Mater.* **2002**, 14, 1806.
(157) Hackey, V.V.; Stoimenov, P.K.; Ho, D.L.; Song, L.P.; Klabunde, K.J.; *J. Appl. Cryst.* 2005, *38*, 619.
(158) Schneider, W.F. *J. Phys. Chem. B*, **2004**, *108*, 273.
(159) Pacchioni, G.; Ricart, J.M.; Illas, F. *J. Am. Chem. Soc.* **1994**, *116*, 10152.
(160) *Science and Technology of Zirconia, Advances in Ceramics, Vol. 3*. A.H. Heuer and L.W. Hobbs (eds.) (The American Ceramics Society, Westerville, OH, 1981).
(161) Steele, B.C.H.; Heinzel, A. *Nature* **2001,** *414*, 345.
(162) Brailsford, A.D.; Logothetis, E.M. *Sensors and Actuators B* **1998**, *52*, 195.
(163) Somov, S.I.; Reinhardt, G.; Guth, U.; Gopel, W. *Solid State Ionics* **2000**, *136-137*, 543.
(164) Stichert, W.; Shüth, F. *Chem. Mater.* **1998**; *10*, 2020.
(165) Howard, C.J.; Kisi, E.; Ohtaka, O. *J. Am. Ceram. Soc.* **1991**, *74*, 2321.
(166) (a) McCullough, J.D.; Trueblood, K.N. *Acta Crystallogr.* **1959**, *15*, 1187. (b) Smith, D.K.; Newkirk, H.W. *Acta Crytallogr.* **1965**, *18*, 982.

(167) Finnis, M.W.; Paxton, A.T.; Methfessel, M.; van Schilfgaarde, M. *Phys. Rev. Lett.* **1998**, *81*, 5149.
(168) Bouvier, P.; Godlewski, J.; Lucazeau, G. *J. Nucl. Mater.* **2002**, *300*, 118.
(169) Gateshki, M.; Petkov, V.; Williams, G.; Pradhan, S.K.; Ren, Y.; *Phys. Rev. B* **2005**, *71*, 224107.
(170) Pacheco, G.; Fripiat, J.J. *J. Phys. Chem. B* **2000**, *104*, 11906.
(171) Mayo, M.J.; Suresh, A.; Porter, W.D. *Rev. Adv. Mater. Sci.* **2003**, *5*, 100.
(172) Xie, S.; Iglesia, E.; Bell, A.T. *Chem. Mater.* **2000**, *12*, 2442.
(173) Srinivasan, R.; Watkins, T.R.; Hubbard, C.R.; Davis, B.H. *Chem. Mater.* **1995**, *7*, 725.
(174)Chang, S.; Doong, R. *Chem. Mater.* **2005**, *17*, 4837.
(175) Chadwick, A.V.; Mountjoy, G.; Nield, V.M.; Poplett, I.J.F.; Smith, M.E.; Strange, J.H.; Tucker, M.G. *Chem. Mater.* **2001**, *13*, 1219.
(176) Boulch, F.; Djurado, E. *Solid State Ionics* **2003**, *157*, 335.
(177) Adachi, G.; Imanaka, N.; Tamura, S. *Chem. Rev.* **2002**, *102*, 2405.
(178) Boulch, F.; Dessemond, L.; Djurado, E. *Solid State Ionics* **2002**, *154-155*, 143.
(179) D. Liu *J. Mater. Sci. Lett.* **1998**, *17*, 467.
(180) Schoonman, J. *Solid State Ionics*, **2000**, *135*, 5.
(181) Mondal, P.; Klein, A.; Jaegermann, W.; Hahn, H. *Solid State Ionics* **1999**, *118*, 331.
(182) Knöner, G.; Reimann, K.; Röwer, R.; Södervall, U.; Schaefer, H. *Proc. Nat. Acad. Sci. U.S.A.* **2003**, *100*, 3870.
(183) Kosacki, I.; Petrovsky, V.; Anderson, H.U. *Appl. Phys. Lett.* **1999**, *74*, 341.
(184) Chen, J.P.; Zhang, X.B.; Tao, X.Y.; Lu, H.M.; Luo, Z.Q.; Liu, F.; *J. Phys. Chem. B* **2006**, *110*, 10348.
(185) Rajh, T.; Chen, L.X.; Lukas, K.; Liu, T.; Thurnauer, M.C.; Tiede, D.M. *J. Phys. Chem. B* **2002**, *106*, 10543.
(186) Schermanz, K. in: *Catalysis by Ceria and Related Materials*; Trovarelli, A. Editor; World Scientific: London, 2002; Chapter 1
(187) Thompson, A.M. *Oxides of the Rare Earths;* Wiley: New York, 1978.
(188) Fujimori, A. *Phys. Rev. B*, **1983**, *28*, 2281.
(189) Wuillioud, E.; Delley, B.; Schneider, W.-D.; Baer, Y. *Phys. Rev. Lett.* **1984**, *53*, 202.
(190) Marabelli, F.; Wachter, P.; *Phys. Rev. B*, **1987**, *36*, 1987.
(191) Koelling, D.D.; Boring, A.M.; Wood, J.H. *Solid State Commun.* **1983**, *47*, 227.
(192) Liu, G.; Rodriguez, J.A.; Chang, Z.; Hrbek, J.; Peden, C.H.F. *J. Phys. Chem. B*, **2004**, *108*, 2931.
(193) Shelef, M.; Graham, G.W. *Catal. Rev. –Sci. Eng.* **1994**, *36*, 433.
(194) Trovarelli, A. *Catal. Rev. Sci.- Eng.* **1996**, *38*, 439.
(195) Martínez-Arias, A.; Fernández-García, M.; Ballesteros, V.; Salamanca, L.N.; Conesa, J.C.; Otero, C.; Soria, J. *Langmuir*, **1999**, *15*, 4797.
(196) Fernández-García, M.; Martínez-Arias, A.; Hungría, A.B.; Iglesias-Juez, A.; Conesa, J.C.; Soria, *Phys. Chem. Chem. Phys.* **2002**, *4*, 2473.
(197) Robinson, R.D.; Spanier, J.E.; Zhang, F.; Chan, S.-W.; Herman, I.P. *J. Applied Physics*, **2002**, *92*, 1936.

(198) Zhang, F.; Chan, S.-W.; Spanier, J.E.; Apak, E.; Jin, Q.; Robinson, R.D.; Herman, I.P. *Appl. Phys. Lett.* **2002**, *80*, 127.
(199) Adachi, G.; Masui, T. In *Catalysis by Ceria and Related Materials*; Trovarelli, A. (Editor); Imperial College Press: London, 2002; Chapter 3.
(200) Rodriguez, J.A.; Wang, X.; Hanson, J.C.; Liu, G.; Iglesias-Juez, A.; Fernández-García, M. *J. Chem. Phys.* **2003**, *119, 5659.*
(201) Kossoy, a.; Feldman, Y.; Wachtel, E.; Gatsman, K.; Lubomirsky, L.; Fleig, J.; Meier, J.; *Phys. Chem. Chem. Phys.* **2006**, *8*, 111.
(202) Di Monte, R.; Kašpar, J.; *Catal. Today*, **2005,** *100*, 27.
(203) Lorschen, C.; Brombley, S.T.; Neyman, K.M.; Illas, F.; *J. Phys. Chem. C* **2007**, *111*, 10142.
(204) Nagai, Y.; Yamamoto, T.; Tanaka, T.; Yoshida, S.; Nonaka, T.; Okamoto, T.; Suda, A.; Sugiura, M. *Catal. Today*, **2002**, *74*, 225.
(205) Chiang, Y.M.; Lavik, E.B.; Kosacki, I.; Tuller, H.L.; Ying, J.Y. *J. Electroceramics*, **1997**, *1*, 7.
(206) Fierro, J.L.G.; Soria, J.; Sanz, J.; Rojo, J.M. *J. Solid State Chem.* **1987**, *66*, 154.
(207) Sohlberg, K.; Pantelides, S.K.; Pennycook, S.J. *J. Am. Chem. Soc.* **2001**, *123*, 6609.
(208) Rodriguez, J.A.; Hanson, J.C.; Kim, J.-Y.; Liu, G.; Iglesias-Juez, A.; Fernández-García, M. *J. Phys. Chem. B,* **2003**, *107, 3535.*
(209) Fu, Q.; Saltsburg, H.; Flytzani-Stephanopoulos, M. *Science*, **2003**, *301*, 935.
(210) Fernández-García, M.; Martínez-Arias, A.; Guerrero-Ruiz, A.; Conesa, J.C.; Soria, J. *J. Catal.* **2002**, *211*, 326.
(211) Vlaic, G.; Di Monte, R.; Fornasiero, P.; Fonda, E.; Kašpar, J.; Graziani, M. *J. Catal.* **1999**, *182*, 378.
(212) Liu, W.; Wadia, C.; Flytzani-Stephanopoulos, M. *Catal. Today*, **1996**, *28*, 391.
(213) Rodriguez, J.A.; Jirsak, T.; Freitag, A.; Hanson, J.C.; Larese, J.Z.; Chaturvedi, S. *Catal. Lett.* **1999**, *62*, 113.
(214) Fu, Q.; Weber, A.; Flytzani-Stephanopoulos, M. *Catal. Lett.* **2001**, *77*, 87.
(215) Shelef, M.; McCabe, R.W. *Catal. Today*, **2000**, *62*, 35.
(216) Colón, G.; Valdivieso, F.; Pijolat, M.; Baker, R.T.; Calvino, J.J.; Bernal, S.; *Catal. Today* **1999**, 50, 271.
(217) Putna, E.S.; Bunluesin, T.; Fan, X.L.; Gorte, R.J.; Vohs, J.M.; Lakis, R.E.; Egami, T. *Catal. Today*, **1999**, *50*, 343.
(218) Yashima, M.; Arashi, H.; Kakihana, M.; Yoshimura, M.; *J. Am. Ceram. Soc.*, **1994**, *77*, 1067.
(219) Kaspar, J.; Fornasiero, P.; Balducci, G.; Di Monte, R.; Hickey, N.; Sergo, V.; *Inorg. Chim. Acta*, **2003**, *349*, 217.
(220) A. Martínez-Arias, M. Fernández-García, A.B. Hungría, J.C. Conesa, G. Munuera, *J. Phys. Chem. B*, **2003**, *107*, 2667.
(221) de Carolis, S.; Pascual, J.L.; Petterson, L.G.M.; Baudin, M.; Wojcik, M.; Hermansson, K.; Palmqvist, A.E.C.; Muhammed, M. *J. Phys. Chem. B*, **1999**, *103*, 7627.
(222) Emsley, J. *The Elements*; Clarendon, Oxford, 1989.
(223) Barr, T.L.; Brundle, C.R. *Phys. Rev. B*, **1992**, *46*, 9199.
(224) Guittet, M.J.; Crocombette, J.P.; Gautier-Soyer, M. *Phys. Rev. B*, **2001**, *63*, 125117.

(225) Bernal, S.; Blanco, G.; Cifredo, G.A.; Delgado, J.J.; Finol, D.; Gatica, J.M.; Rodríguez-Izquierdo, J.M.; Vidal, H.; *Chem. Mater.*, **2002**, *14*, 844.
(226) Wang, X.; Hanson, J.C.; Liu, G.; Rodríguez, J.A. Iglesias-Juez, A.; Fernández-García, M. *J. Chem. Phys.* **2004**, *121, 5434.*
(227) Wang, X.; Rodriguez, J.A.; Hanson, J.C.; Gamarra, D.; Martínez-Arias, A.; Fernández-García, M. *J. Phys. Chem. B,* **2006**, *110*, 428.
(228) Wang, X.; Rodriguez, J.A.; Hanson, J.C.; Gamarra, D.; Martínez-Arias, A.; Fernández-García, M. *J. Phys. Chem. B,* **2005**, *109*, 19595.
(229) Sousa, C.; Illas, F.; *Phys. Rev. B* **1994**, *50*, 13974.
(230) Bosh, H.; Janssen, F.; *Catal. Today* **1988**, *2*, 369.
(231) Forzatti, P.; *Catal. Today* **2000**, *62*, 51.
(232) Hoffman, M.R.; Martin, S.T.; Choi, W.; Bahneman, D.W.; *Chem. Rev.* **1995**, *95*, 69.
(233) Maldoti, A.; Molinari, A.; Amadeni,R.; *Chem. Rev*. **2002**, *102*, 3811.
(234) Johnson, R.W.; Thieles, E.S.; French, R.H.; *Tappi. J.* **1997**, *80*, 233.
(235) Kalyanasendevan, K.; Gratzel, M.; in Optoelectronics Properties of Inorganic Compounds; p. 169-194; Roundhill, D.M.; Fackler, J.P. (Editors); Plenum, New York, 1999.
(236) Bonhole, P.; Gogniat, E.; Gratzel, M.; Ashrit, P.V.; *Thin Solid Films* **1999**, *350*, 269.
(237) Sheveglieri, G. (Editor); *Gas sensors*; Kluwer, Dordrecht, 1992.
(238) Phillips, L.G.; Barbeno, D.M.; *J. Dairy Sci.* **1997**, *80*, 2726.
(239) Selhofer, H.; *Vacuum Thin Films* (August, 1999) 15.
(240) Fujishima, A.; Rao, T.N.; Tryk, D.A.; *J. Photochem. Photobiol. C: Photochem. Rev.* **2000**, *1*, 1.
(241) Zhang, H.-J.; Wang, L.-S.; *J. Am. Chem. Soc.* **2007**, *129*, 3022.
(242) Hu, Z-W.; Kroes, G.-J.; *J. Phys. Chem. B* **2006**, *110*, 8998.
(243) Marchand, R.; Broham, L.; Tournoux, M.; *Mater. Res. Bull.* **1980**, *15*, 1129.
(244) Muscat, J.; Swamy, V.; Harrison, N.M.; *Phys. Rev. B.* **2002**, *65*, 224112.
(245) Yoshitake, H.; Sugahara, H.; Tatsumi, T.; *Phys. Chem. Chem. Phys.* **2003**, *5*, 707.
(246) Zhang, H.; Banfield, J.F.; *J. Phys. Chem. B* **2000**, *104*, 3481.
(247) Depero, L.E.; Sangetti, L.; Allieri, B.; Bontempi, E.; Marino, A.; Zocchi, M.; *J. Cryst. Growth* **1999**, *198/199*, 516.
(248) Lazzeri, M.; Vittadini, A.; Selloni, A.; *Phys. Rev. B* **2001**, *63*, 155409.
(249)Chen, L.X.; Rajh, T.; Wang, Z.; Thurnauer, M.C.; *J. Phys. Chem. B* **1997**, *101*, 10688.
(250)Luca, V.; Djajanti, S.; Howe, R.F.; *J. Phys. Chem. B* **1998**, *102*, 10650.
(251) Yeung, K.L.; Maira, A.J.; Stolz, J.; Hung, E.; Hu, N.K.-C.; Wei, A.C.; Soria, J.; Chao, K.-J.; *J. Phys. Chem. B* **2002,** *106, 4608.*
(252) Steward, S.; Fernández-García, M.; Belver, C.; Mun, B.S.; Requejo, F.G.; *J. Phys. Chem. B* **2006**, *110*, 16482.
(253) Hamad, H.; Catlow, C.R.A.; Woodly, M; Lago, S.; Mejías, L.A.; *J. Phys. Chem. B* **2005**, *109*, 15741.
(254) Chemseddine, A.; Moritz, T.; *Eur. J. Inorg. Chem.* **1999**, 235.
(255) Wang, C.-C.; Ying, J.Y.; *Chem. Mater.* **1999**, *11*, 3133.

(256) Wu, M.; Long, J.; Huang, A.; Luo, Y.; *Langmuir* **1999**, *15*, 8822.
(257) Huang, W.; Tang, X.; Wang, Y.; Kolypin, Y.; Gedankan, A.; *Chem. Comm.* **2000**, 1415.
(258) Yin, H.; Wada, Y.; Kitamura, T.; Kambe, S.; Murasawa, A.; Mori, H.; Sakata, T.; Yangida, S.; *J. Mater. Chem.* **2001**, *11*, 1694.
(259) Aruna, S.T.; Tirosh, S.; Zaban, A.; *J. Mater. Chem.* **2000**, *10*, 2388.
(260) Kominami,H.; Kohno, M.; Kera, Y.; *J. Mater. Chem.* **2000**, *10*, 1151.
(261) Tang, J.; Redl, F.; Zhu, Y.; Siegrist, T.; Brus, L.E.; Steigerwald, M.L.; *Nano Letters* **2005**, *5*, 543.
(262) Exarhos, G.J.; Aloi M.; *Thin Solid Films* **1990**, *193*, 42.
(263) Yanagisawa, K; Ovenstone, J; *J. Phys. Chem. B* **1999**, *103*, 7781.
(264) Inoue, Y.; Yin, S.; Uchida, S.; Fujishiro, Y.; Ishitsura, M.; Min, E.; Sato, T.; *Br. Ceram. Trans.* **1998**, *97*, 222.
(265) Yin, H.; Wadax, X.; Kitamura, T.; Kanbe, S.; Murasawa, S.; Mori H.; Sakata, T.; Yamagida, T.; *J. Mater. Chem.* **2001**, *11*, 1694.
(266) Testino, A.; Bellobono, I.R.; Buscaglia, V.; Canevali, C.; D´Arienzo, M.; Polizzi, S.; Scotti, R.; Morazzoni, F.; *J. Am. Chem. Soc.* **2007**, *129*, 3564.
(267) Ohtani, B.; Ogawa, Y.; Wishimoto, S.; *J. Phys. Chem. B* **1997**, *101*, 3746
(268) Zhang, H.; Banfield, J.F.; *Chem. Mater.* **2002**, *14*, 4145.
(269) Kirsch, B.L.; Richman, E.K.; Riley, A.E.; Tolbert, S.H.; *J. Phys. Chem. B* **2004**, *108*, 12698.
(270) Gateshki, M.; Yin, S.; Ren, Y.; Petkov, V.; *Chem. Mater.* **2007**, *19*, 2512.
(271) Ding, X.Z.; Liu, X.-H.; *J. Mater. Res.* **1998**, *13*, 2556.
(272) Hu, Y.; Tsai, H.-L.; Huang, C.-L.; *Mat. Res. Eng. A.* **2003**, *344*, 209.
(273) Gouma, P.I.; Millis, M.J.; *J. Am. Ceram. Soc.* **2001**, *84*, 619.
(274) Penn, R.L.; Banfield, J.F.; *Am. Mineral.* **1999**, *84*, 1231.
(275) Sakthivel, S.; Kirsch, H.; *Angew. Chem. Int. Ed.* **2003**, *42*, 4908.
(276) Sansonov, G.V.; *The oxide handbook*; IFI/plenum Press, New York, 1982.
(277) Yagi, E.; Hasiguti, R.; *Phys. Rev. B* **1996**, *54*, 7945.
(278) Smith, D.J.; Bursill, L.A.; Blanchin, M.G.; *Philisophical Mag. A* **1984**, *50*, 473.
(279) Knauth, P.; Tuller, H.L.; *J. Appl. Phys.* **1999**, *85*, 897.
(280) Al-Salim, N.I.; Bagshaw, S.A.; Bittar, A.; Kemmit, T.; McQuillan, A.J.; Mills, A.M.; Ryan, M.J.; *J. Mater. Chem.* **2000**, *10*, 2358.
(281) Anpo, M; Takeuchi, M; *J. Catal.* **2003**, *216*, 505.
(282) Shyre, J.J., DeGrure, M.R. *J. Am. Chem. Soc.* **2005**, *127*, 12736.
(283) Kubacka, A.; Fuerte, A.; Martínez-Arias, A.; Fernández-García, M.; *Appl. Catal. B* **2007**, *74*, 26.
(284) Depero, Sagaletti, L., Allieri, B., Bontempi, E., L.E., Marino, A., Zachii, M., *J. Cryst. Growth* **1999**, *198*, 516.
(285) Wang, J.A.; Limas-Ballesteros, R.; López, T.; Moreno, A.; Gómez, R.; Novaro, O.; Bokhim, X.; *J. Phys. Chem. B* **2001**, *105*, 9692.
(286) Adán, C.; Bahamonde-Santos, A.; Fernández-García, M.; Martínez-Arias, A.; *Appl. Catal. B* **2007**, *72*, 11.
(287) Yu, J.C.; Lin, J.; Kwok, R.W.M.; *J. Phys. Chem. B* **1998**, *102*, 5094.

(288) Hernández-Alonso, Coronado, J.M.; Bachiller-Baeza, B.; Fernández-García, M.; Soria, J.; *Chem. Mater.* **2007**, *19*, 4283.
(289) Guidi, V.; Carotta, M.C.; Ferroni, M.; Martinelli, G.; Sacerdoti, M.; *J. Phys. Chem. B* **2003**, *107*, 120.
(290) Mattson, A.; Leideburg, M.; Larsson, K.; Westin, G.; Osterlund, L.; *J. Phys. Chem. B* **2006**, *110*, 1210.
(291) Jeon, M.S.; Yoon, W.S.; Joo, H.; Lee, T.K.; Lee, H.; *Appl. Surf. Sci.* **2000**, *165*, 209.
(292) Fuerte, A.; Hernández-Alonso, M.D.; Maira, A.J.; Martínez-Arias, A.; Fernández-García, M.; Conesa, J.C.; Soria, J.; Munuera, G.; *J. Catal.* **2002**, *212*, 1.
(293) Fernández-García, M.; Martínez-Arias, A.; Fuerte, A.; Conesa, J.C.; *J. Phys. Chem. B.* **2005**, *109*, 6075.
(294) Dai, X.C.; Xiao, H.Y.; Li, W.S.; Na, Y.Q.; *Appl. Catal. A* **2005**, *290,* 25.
(295) Sensato, F.R.; Custodio, R.; Longo, E.; Beltrán, A.; Andrés, J.; *Catal. Today* **2003**, *85*, 145.
(296) Fresno, F.; Tudela, D.; Coronado, J.M.; Fernández-García, M.; Hungría, A.; Soria, J.; *Phys. Chem. Chem. Phys.* **2006**, *8*, 2421.
(297) Depero, L.E; Marino, A.; Allieri, B.; Bontempi, E.; Sangaletti, L.; Casale, C.; Notaro, M.; *J. Mater. Res.* **2000**, *15*, 2080.
(298) Fuerte, A.; Hernández-Alonso, M.D.; Maira, A.J.; Martínez-Arias, A.; Fernández-García, M.; Conesa, J.C.; Soria, J.; *Chem. Comm.* **2001**, 2178.
(299) Xu, A.-W.; Gao, Y.; Liu, H.-Q.; *J. Catal.* **2002**, *207*, 151.
(300) Klingshirn, C.; *Phys. Stat. Sol.* **2007**, *244*, 3027.
(301) Dransfield, G.P.; *Rad. Protection Dosimetry* **2000**, *91*, 271.
(302) Fan, J.; Freer, R.; *J. Appl. Phys.* **1995**, *77*, 4795.
(303) Colón-Ibañez, G.; Belver, C.; Fernández-García, M.; *Nanostrcuctured oxides in Photo-catalysis* in "Synthesis, Properties and Applications of Oxide Nanoparticles" (Rodríguez, J.A., Fernández-García, M; Eds.). Whiley: N. J., 2007. Chpt. 14.
(304) Wang, Z.L.; *J. Phys. Condens. Matter* **2004**, *16*, R829.
(305) Wu, X.; Jiang, P.; Ding, Y.; Cai, W.; Xie, S.S.; Wang, Z.L.; *Adv. Mater.* **2007**, *19*, 2319.
(306) Yadar, H.K.; Gupta, V.; Sreeniva, K.; Singh, S.P.; Sundarakannan, B.; Katiyar, R.S.; *Phys. Rev. Lett.* **2006**, *97*, 085502.
(307) Jin, L.; Xu, Z.; Shang, J.; Sun, X.; Guo, H.; *Mater. Sci. Eng. A* **2002**, *332*, 356.
(308) Wang, Y.S.; Thomas, P.J.; O´Brien, P.; *J. Phys. Chem. B* **2006**, *110*, 21412.
(309) Cornell, R.M.; Schwertmann, U. "The iron oxides" (VCH; Weinheim, 1996).
(310) Weiss, W.; Ranke, W.; *Prog. Surf. Sci.*, **2002**, *70*, 151.
(311) Feltin, N.; Pileni, M.P.; *Langmuir*, **1997**, *13*, 3927.
(312) Morales, M.P.; Pecharroman, C.; Conzales Carreño, T.; Serna, C.J.; *J. Sol. State Chem.*, **1994**, *108*, 158.
(313) Moreno, E.M.; Zayat, M.; Morales, M.P.; Serna, C.J.; Roig, A.; Levi, D.; *Langmuir*, **2002**, *18*, 4972.
(314) Jolivet, J.J.; Chaneac, C.; Tronc, E.; *Chem. Comm.*, **2004**, 472
(315) Chen, L.X.; Liu, T.; Thurnauer, M.; Csenesits, R.; Rajh, T.; *J. Phys. Chem. B* **2002**, *106*, 8539.

(316) Corrias, A.; Ennas, G.; Montjoy, G.; Paschina, G.; *Phys. Chem. Chem. Phys.*, **2000**, *2*, 1045.
(317) Lu, L.; Li, L.; Wang, X.; Li, G.; *J. Phys. Chem. B* **2005**, *109*, 17151.
(318) Ennas, G.; Marongini, G.; Musini, A.; Falqui, A.; Belliarano, P.; Camini, R.; *J. Mater. Res.*, **1999**, *14*, 1570.
(319) Chanéac, C.; Tronc, E.; Jolivet, J.P.; *Nanostruct. Mater.*, **1995**, *6*, 715.
(320) Larcher, D.; Masquelier, C.; Bonnin, D.; Chabre, Y.; Masson, V.; Leriche, J.B.; Tarasxob, J.M.; *J. Electrchem. Soc.* **2003**, *150*, A133.
(321) Diéguez, A.; Romano-Rodríguez, A.; Vilá, A.; Morante, J.R.; *J. Appl. Phys.* **2001**, *90*, 1550.
(322) Jones, F.H.; Dixon, R.; Foord, J.S.; Egdell, R.G.; Pethica, J.B. *Surf. Sci.* **1997**, *376*, 367.
(323) Cox, D.F.; Fryberger, T.B.; Semancik, S. *Phys. Rev. B* **1988**, *38*, 2072.
(324) Manassidis, I.; Goniakovski, J.; Kantorovich, L.N.; Gillan, M.J. *Surf. Sci.* **1995**, *339*, 258.
(325) Fröhlich, D.; Klenklies, R.; Helbig, R. *Phys. Rev. Lett.* **1978**, *41*, 1750.
(326) Samson, S.; Fonstad, C.G. *J. Appl. Phys.* **1973**, *44*, 4618.
(327) Bläser, G.; Rühl, Th.; Diehl, C.; Ulrich, M.; Kohl, D. *Phys. A* **1999**, *266*, 218.
(328) Centi, G.; Trifiro, F. *Catal. Rev.* **1986**, *28*, 165.
(329) Popescu, D.A.; Herrmann, J.-M.; Ensuque, A.; Bozon-Verduraz, F. *Phys. Chem. Chem. Phys.* **2001**, *3*, 2522.
(330) Kennedy, M.K.; Kruis, F.E.; Fissan, H.; Mehta, B.R.; Stappart, S.; Dumpich, G.; *J. Appl. Phys.* **2003**, *93*, 551.

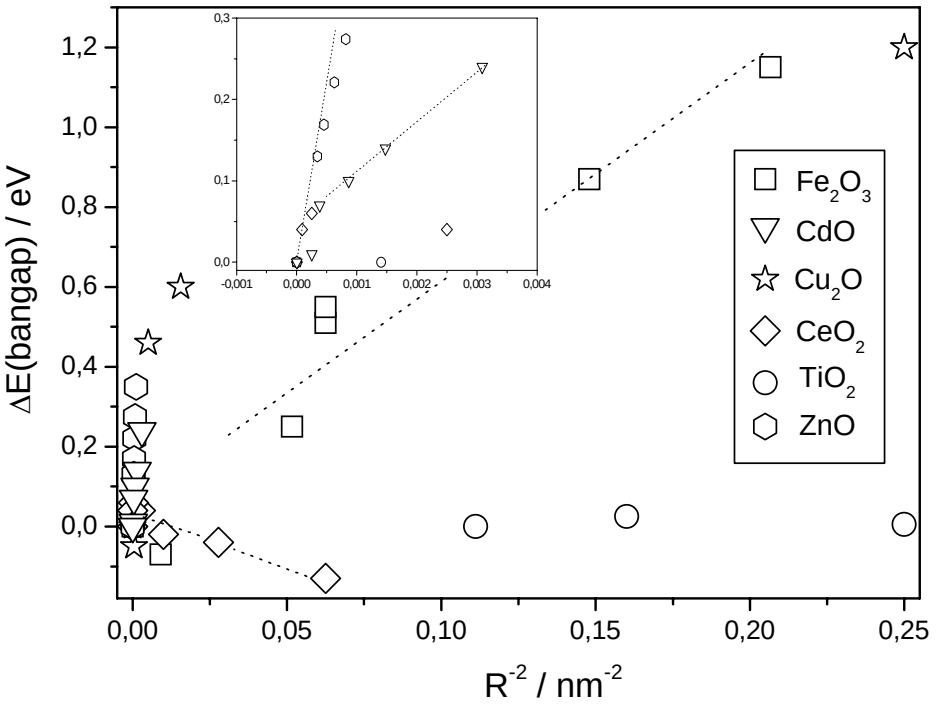

Fig. 1. Optical band gap energy as a function of the inverse squared primary particle size for several metal oxides.

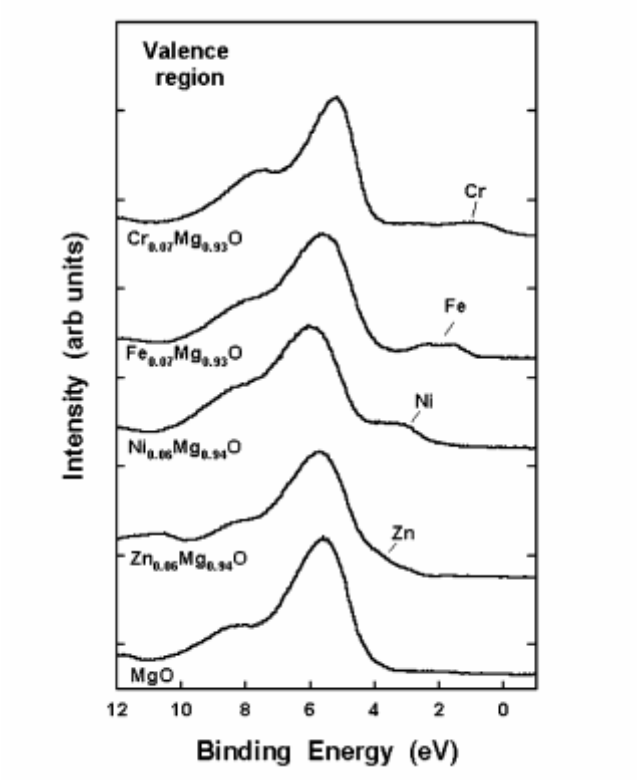

Figure 2 Valence photoemission spectra for pure and doped magnesium oxide (adapted after ref. [140]).

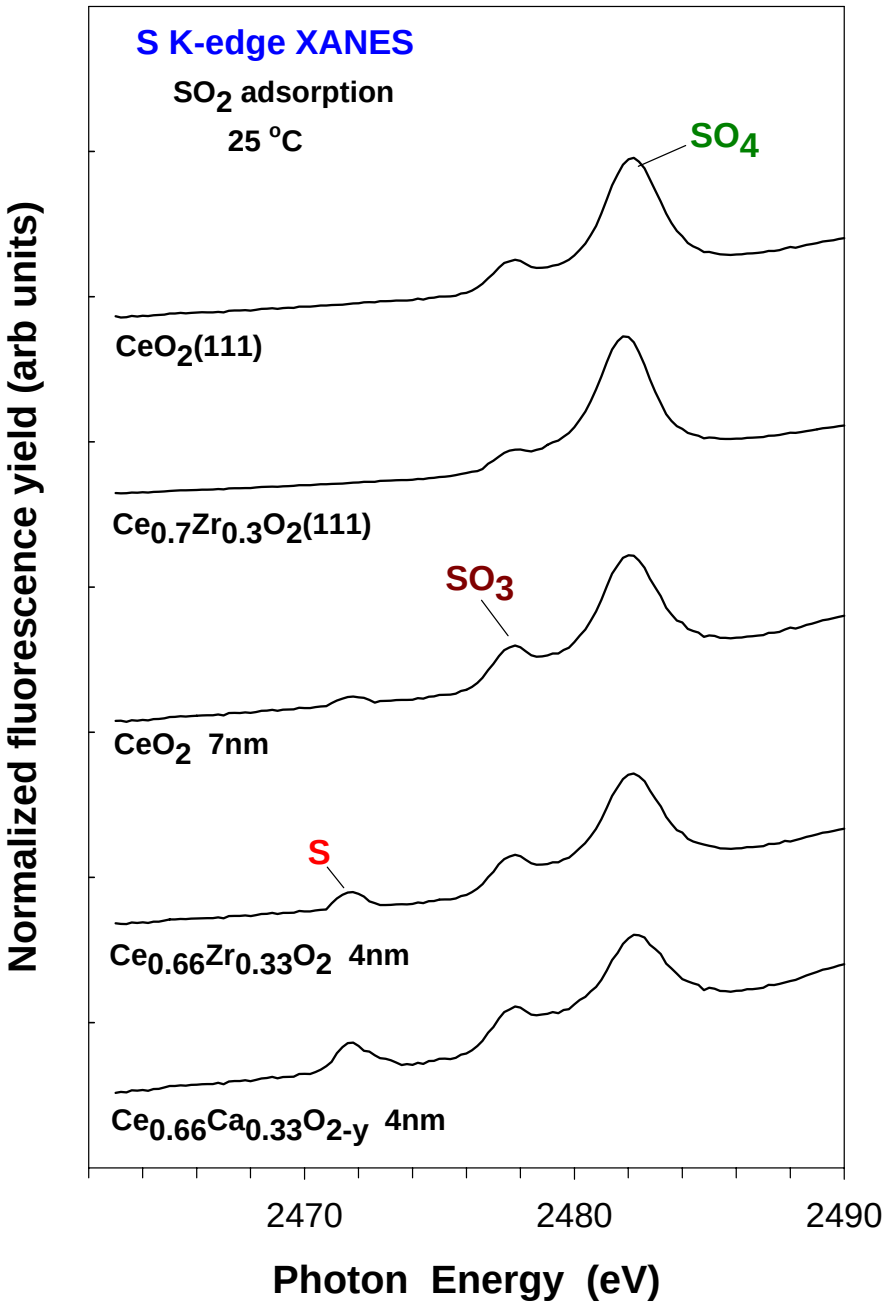

Figure 3 S K-edge XANES spectra recorded after adsorbing SO_2 on extended surfaces and nanoparticles of pure and doped ceria (adapted after ref. [50]).